Journal of Medicinal Chemistry

pubs.acs.org/jmc

Article

Interplay among Conformation, Intramolecular Hydrogen Bonds, and Chameleonicity in the Membrane Permeability and Cyclophilin A Binding of Macrocyclic Peptide Cyclosporin O Derivatives

Dongjae Lee, Sungjin Lee, Jieun Choi, Yoo-Kyung Song, Min Ju Kim, Dae-Seop Shin, Myung Ae Bae, Yong-Chul Kim, Chin-Ju Park,* Kyeong-Ryoon Lee,* Jun-Ho Choi,* and Jiwon Seo*

Cite This: *J. Med. Chem.* 2021, 64, 8272−8286

Read Online

ACCESS | Metrics & More | Article Recommendations | Supporting Information

ABSTRACT: A macrocyclic peptide scaffold with well-established structure−property relationship is desirable for tackling undruggable targets. Here, we adopted a natural macrocycle, cyclosporin O (**CsO**) and its derivatives (**CP1**−**3**), and evaluated the impact of conformation on membrane permeability, cyclophilin A (CypA) binding, and the pharmacokinetic (PK) profile. In nonpolar media, **CsO** showed a similar conformation to cyclosporin A (**CsA**), a well-known chameleonic macrocycle, but less chameleonic behavior in a polar environment. The weak chameleonicity of **CsO** resulted in decreased membrane permeability; however, the more rigid conformation of **CsO** was not detrimental to its PK profile. **CsO** exhibited a higher plasma concentration than **CsA**, which resulted from minimal CypA binding and lower accumulation in red blood cells and moderate oral bioavailability (F = 12%). Our study aids understanding of **CsO**, a macrocyclic peptide that is less explored than **CsA** but with greater potential for diversity generation and rational design.

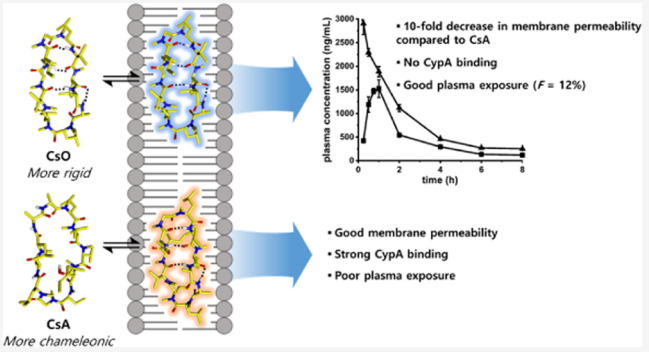

INTRODUCTION

An intracellular protein−protein interaction (PPI) is a general process that transmits cellular signaling. The desired epitope binds to the surface of the target protein, and the subsequent function is regulated. For decades, intracellular PPIs have been considered to be intractable as drug targets for conventional modalities such as small molecules.[1−3] A large surface area is often required to facilitate interactions between a compound and the surface of a target protein and to inhibit PPIs.[4,5] Although antibodies specifically recognize the large surface areas of proteins, they are mostly limited to extracellular targets due to their lack of membrane permeability. Between small molecules and antibodies, macrocyclic peptides belong to an intermediate chemical space, often called the beyond rule of 5 (bRo5) space.[6,7] Macrocyclic peptides are considered a promising molecular platform for regulating intracellular PPIs. Interactions with high affinity and specificity are expected because macrocyclic peptides can readily adopt the raw sequences and conformations of peptide epitopes,[8−10] which are the core domains that inhibit PPIs. The preorganized structure of macrocyclic peptides decreases the entropic cost of binding.[11] In addition, macrocyclic peptides often exhibit resistance to proteolytic degradation[12] and show improved membrane permeability.[13]

In the bRo5 space, the structural features of highly membrane-permeable natural products such as cyclosporin A (**CsA**),[14] griselimycin,[15] sanguinamide A,[16] and phepropeptins[17] have been investigated. In these peptides, lipophilic amino acids (e.g., Leu, Val, Pro, Ile, and Phe) are dominant, and the polar amide backbone is masked by *N*-methylation, intramolecular hydrogen bonds, or β-branched side chains to reduce the polar surface area (PSA) or the solvent-accessible surface area (SASA).[18,19] Following natural design principles, synthetic macrocyclic peptides have been investigated employing *N*-methylation/alkylation,[20−23] stereoisomerization,[17,24,25] side-chain variations,[16,21,26,27] or the protection of functional groups[28,29] on diverse peptide scaffolds,[14,16,18,30] and some of these peptides showed remarkable membrane permeability and oral bioavailability. Structure−permeability relationship (SPR) studies have identified the relevant factors that influence membrane permeability. Plots of permeability versus lipophilicity (AlogP) for macrocyclic peptides show a binomial distribution,[21] which is observed irrespective of ring size up to undecamer cyclosporine derivatives.[31] Increased molecular

Received: February 4, 2021
Published: June 7, 2021

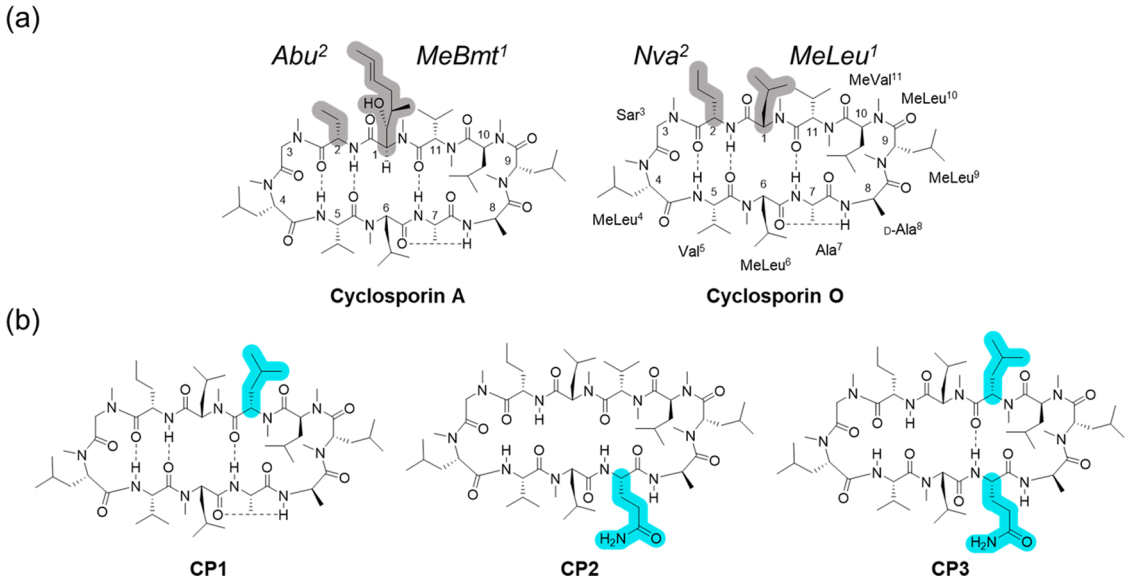

Figure 1. (a) Structures of cyclosporin A (**CsA**) and cyclosporin O (**CsO**). (b) Derivatives of **CsO** (**CP1−3**) are shown. The substituted side chains are highlighted in cyan.

weight has adverse effects, decreasing permeability by an order of magnitude due to the increased PSA.[32] Intramolecular hydrogen bonds or *N*-methylation patterns had no consistent effect on permeability,[33] even though they are essential for masking the polar amide backbone; thus, a general guideline for the numbers or positions of *N*-methylation in the macrocyclic peptide backbone is still difficult to establish. However, it is now accepted that favorable conformational features that permit membrane permeation are intramolecular hydrogen bonds and a reduced SASA, which are obtained by masking amide protons (e.g., β-turns and β-sheets) in a low dielectric medium.[13,19,22,23,27,33,34]

Recently, some macrocyclic compounds with high membrane permeability have been shown to exhibit conformational changes depending on the environmental polarity.[19,35,36] These chameleonic macrocycles favor an "open" conformation in aqueous environments by exposing polar groups toward the exterior to interact with water molecules and increase aqueous solubility, while a "closed" conformation is predominantly adopted in hydrophobic environments to shield the polar backbone with intramolecular hydrogen bonds or lipophilic side chains, leading to improved membrane permeability. Therefore, molecular chameleonicity helps a macrocycle reach an optimal solubility and membrane permeability by balancing open and closed conformations, respectively.[37] Chameleonicity has been observed in synthetic and natural membrane-permeable cyclic peptides.[16,38−41] This unique conformational behavior has been experimentally monitored by NMR[42] and circular dichroism (CD)[39] spectroscopic techniques in polar and lipophilic media and computationally simulated in various models.[35,36] Among the chameleonic macrocycles, **CsA** is a prime example and has been thoroughly studied for its exceptional oral bioavailability compared with similarly sized peptides. Cyclosporines are natural metabolites produced by fungi, and 25 cyclosporines have been isolated thus far.[43] Most cyclosporines contain the unusual amino acid (4*R*)-4-[(*E*)-2-butenyl]-4-methyl-L-threonine (MeBmt) at position 1 and exhibit biological activities such as immunosuppression or antifungal activity. The amino acid MeBmt is mostly responsible for the unique structural and biological properties of **CsA**; however, it is also a major reason for the difficulty that has been encountered during the expansion of the cyclosporine derivative library because of the long synthetic routes required to obtain MeBmt[44−48] and the low yields observed during sequence elongation with the MeBmt residue.[49,50] Instead, semisynthetic routes have been used to prepare cyclosporine derivatives avoiding the chemical synthesis of MeBmt.[51−53] Cyclosporin O (**CsO**) is a unique member of the cyclosporine family that does not contain the MeBmt residue and has attracted relatively little interest due to its lack of noticeable biological function compared to MeBmt-containing cyclosporines; therefore, only a few synthetic methods[54−58] and biological functionalities[43] (e.g., immunosuppressive activity and antifungal activity) have been reported. However, the absence of the MeBmt residue makes **CsO** an attractive scaffold for the expansion of the cyclosporine library in the intermediate chemical space.

Recently, a major effort has been focused on the establishment of the structure−property relationship of macrocyclic peptides in the bRo5 space. In particular, for macrocycles with molecular weights above 1000 Da, a far better understanding of the features that influence membrane permeability and drug-likeness is essential, which will eventually lead to the development of a general tool for the prediction of membrane permeability in this underexplored chemical space. The main purpose of this study was to establish the conformation-permeability relationship of **CsO** and its derivatives compared to that of **CsA** and to evaluate the potential utility of **CsO** scaffolding for peptide drug design. First, we optimized the synthesis of macrocyclic peptide scaffolds based on **CsO** and its derivatives (**CP1−3**). Then, we investigated their structural characteristics, membrane permeability, and cyclophilin A (CypA) binding. Molecular modeling and NMR spectroscopy showed a similar conformation in nonpolar environments for **CsA** and **CsO**, but **CsO** had reduced chameleonic behavior in polar environments compared to **CsA**. The membrane permeability of the cyclic peptides was evaluated using a parallel artificial membrane permeability assay (PAMPA) and a Caco-2 assay, and correlations among conformation, intramolecular hydrogen bonds, chameleonicity, and membrane

https://doi.org/10.1021/acs.jmedchem.1c00211
J. Med. Chem. 2021, 64, 8272−8286

Scheme 1. Synthesis of CsO Derivatives

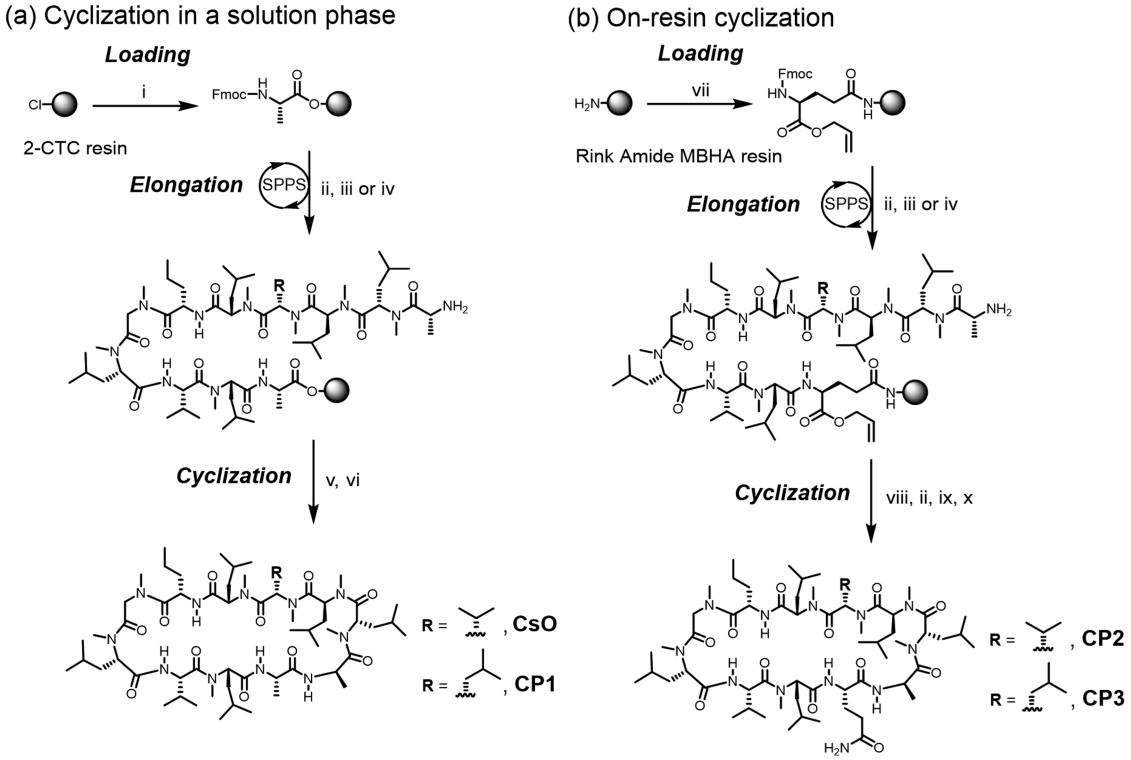

*Reaction conditions: (i) Fmoc-Ala-OH, DIEA, CH_2Cl_2, rt, 5 h; (ii) 20% piperidine in dimethylformamide (DMF), rt, 5 min; (iii) Fmoc-AA-OH, HATU, DIEA, DMF, microwave, 75 °C, 10 min; (iv) Fmoc-MeLeu-OH, HOAt, DIC, DIEA, DMF, microwave, 75 °C, 20 min (×2); (v) TFA/TIS/CH_2Cl_2 95:2.5:2.5, rt, 10 min (×2); (vi) HATU, DIEA, DMF, microwave, 75 °C, 10 min; (vii) Fmoc-Glu-OAll, HATU, DIEA, DMF, microwave, 75 °C, 10 min; (viii) $Pd(PPh_3)_4$, $PhSiH_3$, CH_2Cl_2, rt, 3 h; (ix) PyBOP, HOAt, DIEA, CH_2Cl_2, rt, 2 h; (x) TFA/TIS/CH_2Cl_2 95:2.5:2.5, rt, 2 h.

permeability were investigated. Moreover, a pharmacokinetic (PK) study was carried out on mice to evaluate plasma concentrations and oral bioavailability. Discrepancies between the PK profiles of **CsA** and **CsO** were explained by the results from the CypA binding assay and a blood-to-plasma partition experiment. Our results provide a deeper understanding of **CsO**, an attractive macrocyclic scaffold for the diversity generation, as well as insights into the relationship between conformational chameleonicity (or rigidity) and permeability among cyclosporine macrocycles.

RESULTS

Design and Synthesis. In **CsA**, MeBmt[1] and Abu[2] residues are crucial for binding with cyclophilin and then calcineurin, leading to well-known immunosuppressive activity.[48] **CsO** is a unique cyclosporine that does not contain the MeBmt[1] residue (Figure 1a) and is potentially a suitable scaffold to investigate biological activities without unwanted immunomodulatory activity.[43,47,59] Understanding the conformational effect of amino acid substitutions on the **CsO** scaffold, in comparison to the unique structural characteristics of **CsA**, is a prerequisite for the application of **CsO**. As shown in Figure 1b, three derivatives of **CsO** were prepared. It was reported that [MeLeu[11]] CsA possessed a practically identical conformation to **CsA**, as determined by X-ray crystallography.[48] Moreover, the replacement of MeVal with MeLeu in a cyclosporine sequence provided a much improved coupling efficiency due to the lower steric hindrance (e.g., coupling of MeLeu[10] onto MeVal[11]). [MeLeu[11]] CsO or **CP1** was designed to generate a scaffold with less synthetic difficulty. To carry out an on-resin cyclization, Ala[7] was replaced with glutamine, which can be used as an anchoring residue on a solid resin (**CP2** and **CP3**). In addition, **CP2** and **CP3** enabled us to evaluate the effects of polar amino acid incorporation, such as glutamine, on membrane permeability.[29] We suggest the macrocyclic scaffold **CP3**, which can be synthesized on-resin and exhibits a good coupling efficiency between MeVal[11] and MeLeu,[10] can be suitable for the generation of a large library of compounds.

Several synthetic methods have been reported for **CsO**: a fragment-based synthesis,[58] a solution-phase synthesis,[55,56] and an on-resin synthesis with long coupling times[60] or with a strong coupling reagent, bis(trichloromethyl) carbonate (BTC).[54,57] In this work, the linear sequences of **CsO** and its derivatives were synthesized via a standard Fmoc/*t*Bu solid-phase peptide synthesis (SPPS) protocol under microwave irradiation (Scheme 1). Due to severe steric hindrance by the *β*-branched side chain, the peptide coupling of MeLeu[10] onto MeVal[12] was performed twice using *N*,*N*′-diisopropylcarbodiimide (DIC)/HOAt. The desired linear undecapeptide was cleaved from the solid support by a trifluoroacetic (TFA) cocktail (TFA/TIS/CH_2Cl_2 95:2.5:2.5). Without purification, macrocyclization was carried out in a solution phase under microwave irradiation with the addition of *N*,*N*-diisopropylethylamine (DIEA) followed by 1-[bis-(dimethylamino)-methylene]-1*H*-1,2,3-triazole[4,5-*b*]pyridinium 3-oxide hexafluorophosphate (HATU; **CsO** and **CP1** in Scheme 1a). It should be noted that the coupling reaction of MeLeu[10] onto

https://doi.org/10.1021/acs.jmedchem.1c00211
J. Med. Chem. 2021, 64, 8272−8286

MeVal[11] was attempted under various conditions, such as through the use of HATU, PyBOP, PyBrOP, PyClOP, TFFH, COMU, DIC/HOBt, and Fmoc-MeLeu-Cl at both room temperature and an elevated temperature (75 °C). None of the above conditions resulted in satisfactory coupling efficiency, demonstrating the superiority of DIC/HOAt conditions in this type of sterically demanding coupling reaction (84% conversion).

On-resin macrocyclization for **CP2** and **CP3** (Scheme 1b) was attempted employing various coupling reagents, such as uroniums, phosphoniums, carbodiimides, or acyl halides. In the initial screening of the coupling reagents, HOAt appeared to be crucial. In the presence of HOAt, macrocyclization conditions were surveyed and optimized as PyBOP/HOAt/DIEA in CH_2Cl_2 for 2 h (entry 8 in Table 1). Interestingly, CH_2Cl_2 worked better than DMF or other solvents, as shown in entries 3–6 (DIC/HOAt system) and in entries 7–9 (PyBOP/HOAt system). Reaction times longer than 2 h did not increase product yield under these conditions. The crude product was purified by preparative reverse-phase high-performance liquid chromatography (RP-HPLC), and the desired products were obtained at a 2–7% overall yield depending on the sequence. Although racemization in macrocyclization was observed by HPLC and liquid chromatography–mass spectrometry (LC-MS), the isomer was separated by preparative RP-HPLC.

Table 1. Conditions for the On-Resin Macrocyclization of CP3[a]

entry	coupling reagent	base	solvent	time	conversion (%)[a]	purity (%)[a]
1	HATU/HOAt	DIEA	DMF	2	95[b]	9
2	HATU/HOAt	DIEA/4-DMAP	DMF/DCE 2:8	2	95[b]	8
3	DIC/HOAt	DIEA	DMF	2	49	nd[c]
4	DIC/HOAt	DIEA	DMF/CH_2Cl_2 8:2	2	46	nd[c]
5	DIC/HOAt	DIEA	CH_2Cl_2	2	53	7
6	DIC/HOAt	DIEA	CH_3CN	2	19	nd[c]
7	PyBOP/HOAt	DIEA	NMP	2	46	7
8	PyBOP/HOAt	DIEA	CH_2Cl_2	2	94[b]	15
9	PyBOP/HOAt	DIEA	CH_3CN	2	15	nd[c]
10	PyBOP/HOAt	collidine	CH_2Cl_2	2	81[b]	3
11	PyAOP/HOAt	DIEA	CH_2Cl_2	2	95[b]	9

[a]On-resin macrocyclization was performed by adding coupling reagent (4.0 equiv) and base (10.0 equiv) in solvent (1 mL) into the resin (2.5 μmol). [a]Conversion and purity of a crude sample were evaluated by HPLC monitored at 220 nm. [b]Conversion was determined by an integrated area on an extracted ion chromatogram (EIC) by LC-MS. [c]nd, product not detected.

Conformational Investigation Using Two-Dimensional (2D) NMR Spectroscopy. The conformations of **CsO** and **CP1–3** in a nonpolar environment were investigated by 2D NMR spectroscopy. Nuclear Overhauser effect spectroscopy (NOESY) spectra in chloroform demonstrated patterns of transannular hydrogen bonds in cyclic peptides. **CsO** and **CP1** showed the same NOE peaks of $9H_\alpha$–$10H_\alpha$, 2NH–5NH, and 7NH–11NMe, as seen in **CsA** (Figures 2, S3, S5, and S7).[61] In **CsA**, these NOE peaks were well characterized: $9H_\alpha$–$10H_\alpha$ indicates a 9–10 *cis*-amide bond; 2NH–5NH indicates a rigid β-sheet with hydrogen bonds of 2NH–5CO and 5NH–2CO; and 7NH–11NMe indicates a flexible loop including a hydrogen bond of 7NH–11CO. The similar NOE cross-peaks of **CsA**, **CsO**, and **CP1** strongly support the conclusion that the cyclic peptides exist as closed backbone conformations in nonpolar media. In **CsA**, MeVal[11] to MeLeu[11] substitution was reported to have a minimal effect on backbone conformation,[48] which was also the case in **CsO**, demonstrating identical transannular interactions between **CsO** and **CP1**.

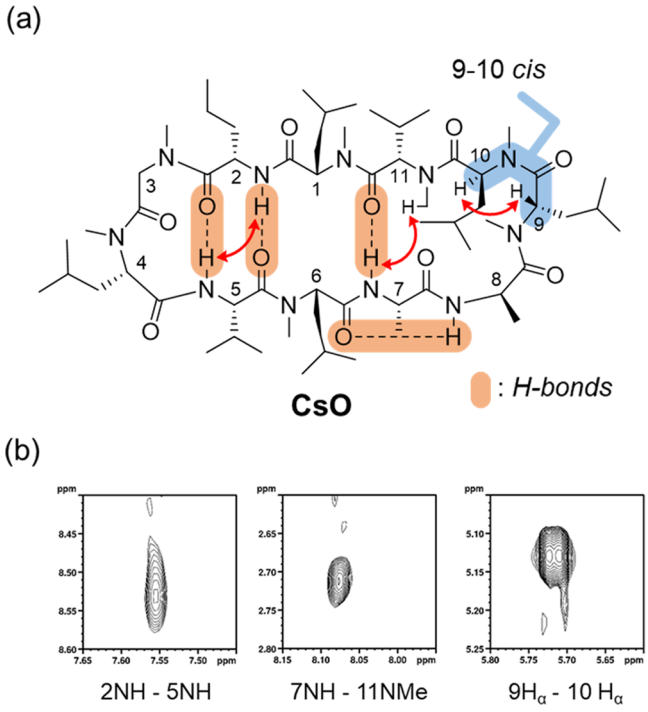

Figure 2. (a) Structural features of the backbone of **CsO**. Red arrows indicate significant transannular interactions confirmed by NOESY. (b) Cross-peaks on the NOESY spectra used to calculate the conformation of **CsO**.

Ala[7] to Gln[7] substitution resulted in different conformational effects disrupting the intramolecular hydrogen-bond patterns in **CP2** and **CP3**. For **CP2**, only a 9–10 *cis*-amide bond was identified without any NOE signal of transannular interaction (Figure S9). The NOESY spectra of **CP3** showed a 9–10 *cis*-amide bond and one transannular hydrogen bond of 7NH–11CO (Figure S11) indicating substitution of MeVal[11] by MeLeu[11] resulted in the shielding of backbone amides from solvent and more constrained backbone conformation in the hydrophobic environment.[16] Hydrogen-bond patterns related to a rigid β-sheet (e.g., 2NH–5CO and 5NH–2CO) were all lost in **CP2** and **CP3**. Taken together, these results show that **CsA**, **CsO**, and **CP1** had similar transannular interactions and similar backbone conformations, and much more heterogeneous conformations were suggested for **CP2** and **CP3** in a nonpolar environment.

Conformational Investigation Using One-Dimensional (1D) NMR Spectroscopy. Further hydrogen-bonding and shielding patterns were investigated with variable-temperature

https://doi.org/10.1021/acs.jmedchem.1c00211
J. Med. Chem. 2021, 64, 8272–8286

(VT) and hydrogen-deuterium exchange (HDX) NMR spectroscopy (Figures S12 and S13). VT NMR provides an indirect measure of hydrogen-bond strength with temperature coefficient values.[62] All amide protons in **CsA**, **CsO**, and **CP1** showed similar patterns of temperature coefficients, supporting similar backbone conformations of the three peptides (Table 2). For **CP2** and **CP3**, distinct and larger temperature coefficient values were obtained than those for **CsA**, **CsO**, and **CP1**. Generally, temperature coefficients larger than (or more positive than) −4.6 ppb/K are indicators of hydrogen bonds.[62] However, amides in poorly defined regions often had temperature coefficient values larger than −4.6 ppb/K. Previously reported cyclic peptides with no intracellular hydrogen bond,[17,26,39] including Li-complexed **CsA**,[63] belong to this exception. Amide protons in **CP2** and **CP3** are in heterogeneous conformation, as demonstrated by 2D NMR, and temperature coefficient values provided additional evidence that the conformations of **CP2** and **CP3** are distinct from those of **CsA**, **CsO**, and **CP1**. Although the patterns of the temperature coefficient are similar, hydrogen/deuterium exchange (HDX) NMR spectroscopy data showed different patterns of solvent accessibility and half-life of amide protons in **CsA**, **CsO**, and **CP1**.[26] The longest half-life was observed for 7NH in **CsA** ($t_{1/2}$ = 2800 min) and for 5NH in **CsO** and **CP1** ($t_{1/2}$ = 2700 and 5200 min, respectively). The half-lives of 8NH in **CsO** and **CP1** were relatively short compared to that in **CsA**, indicating an exposure of 8NH to bulk solvent. Although 2D NOESY and VT NMR data indicated similar backbone conformations for **CsA**, **CsO**, and **CP1**, the latter two exhibited different shielding patterns from those of **CsA**. The large side chain of **CsA**, MeBmt, mainly shielded the environment of 7NH,[61] but the β-sheet conformation formed by 2NH and 5NH could be well maintained and stabilized in **CsO** and **CP1**. In contrast with **CsA**, **CsO**, and **CP1**, the lack of conformational homogeneity in **CP2** and **CP3** was demonstrated by broad 1D NMR amide proton peaks (Figure S12). These Gln[7]-substituted cyclic peptides exhibited different temperature coefficients and HDX patterns (Table 2), and the backbone amide protons are more exposed on the exterior of the molecule and accessible to solvent molecules.

Table 2. Temperature Coefficients and Half-Lives of CsO Derivatives

	temperature coefficient ($\Delta\delta/\Delta T$, ppb/K)[a]				
amide proton	**CsA**	**CsO**	**CP1**	**CP2**	**CP3**
2NH	**−3.04 (−3.6)**	**−3.66**	**−4.22**	−1.88	−3.86
5NH	−1.58 (−1.8)	−1.40	−1.54	−1.82	−1.42
7NH	**−3.78 (−3.6)**	**−3.20**	**−3.10**	−2.60	−1.06
8NH	−1.02 (−1.1)	−2.30	−1.66	−0.94	−0.26
	Half-Life ($t_{1/2}$, min)[b]				
2NH	520	2100	3500	610	480
5NH	1200	**2700**	**5200**	720	730
7NH	**2800**	700	1000	200	80
8NH	930	320	390	50	60

[a]Temperature coefficients were calculated from NMR spectra obtained in $CDCl_3$ between 298 and 313 K. Values in parentheses are previously reported values.[63] [b]Half-lives were determined by a hydrogen-deuterium exchange (HDX) experiment, which was carried out in $CDCl_3$ with 10% (v/v) CD_3OD. CD_3OD was used as a deuterium source. Peptides were lyophilized repeatedly, at least three times, and each sample contained a minimal amount of TFA, in the range of 0.0001−0.0005% by volume (Figure S14).

Conformational Investigation via Molecular Simulation. Prediction of the conformation of macrocyclic peptides containing *N*-methylated backbone amides or noncanonical amino acids has presented unique challenges. The absence of amide protons limits the use of dihedral constraints, and the intrinsic patterns of noncanonical amino acids in NMR spectra are complicated. Recently, Lokey and co-workers reported a refined workflow to predict the conformation of *N*-methylated cyclic hexapeptides using molecular dynamics simulations and quantum mechanical calculations, which was termed the conformational analysis from NMR and density functional prediction of low-energy ensembles (CANDLE) method.[65] Applying the CANDLE method, we performed a conformational investigation of undecameric cyclic peptides, **CsO** and their derivatives (**CP1**−**3**). Initially, the conformational determination of **CsA** was carried out to examine whether the CANDLE method was valid for the undecameric cyclic peptides (a detailed workflow using the CANDLE method for the prediction of **CsA** conformation is provided in the SI). Then, the computationally generated **CsA** conformation was compared to experimental structures determined by X-ray crystallography (Figure 3a).[64] Population-weighted average values of dihedral angles and hydrogen-bond distances were similar to those of the crystal structure and the solution structure identified in $CDCl_3$ (Tables S10−S12); therefore, we moved on to carry out conformational predictions of **CsO** and **CP1**−**3**.

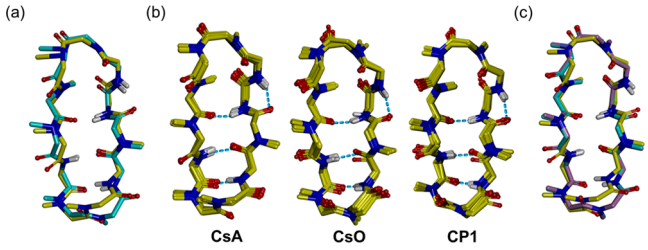

Figure 3. (a) Overlay of crystal structure (cyan, CSD: DEKSAN)[64] and the lowest-energy conformer of **CsA** calculated by CANDLE (yellow). (b) Calculated ensemble of the conformations of **CsA**, **CsO**, and **CP1** visualized via Discovery Studio v.17.1. The cyan dashed line indicates hydrogen bonds. (c) Overlay of the lowest-energy conformers of **CsA** (yellow), **CsO** (cyan), and **CP1** (magenta). Side chains are omitted for clarity.

CsO shares similar structural features with **CsA**, such as ring size, *N*-methylation pattern, D-/L-configuration, and hydrophobic side chains. Based on the CANDLE protocol used for **CsA**, conformational ensembles for **CsO** and **CP1** were obtained (Figure 3b). The transannular hydrogen-bonding interactions were used as constraints to generate conformational ensembles of **CsO** and **CP1**: 2NH−5NH, 7NH−11NMe, and $9H_\alpha$-$10H_\alpha$. Similar to **CsA**, **CsO** showed a backbone conformation composed of an antiparallel β-sheet (MeLeu[1]−MeLeu[6]), a flexible loop (D-Ala[8]−MeLeu[1]), and an inverse γ-turn (MeLeu[6]−D-Ala[8]).[64] The additional hydrogen bond of 8NH-6CO, which was not applied as a constraint during calculations, was identified in the ensemble conformations. The dihedral angles of each amino acid and significant intramolecular distances were compared between **CsA** and **CsO**, and a similar backbone conformation was confirmed

https://doi.org/10.1021/acs.jmedchem.1c00211
J. Med. Chem. 2021, 64, 8272−8286

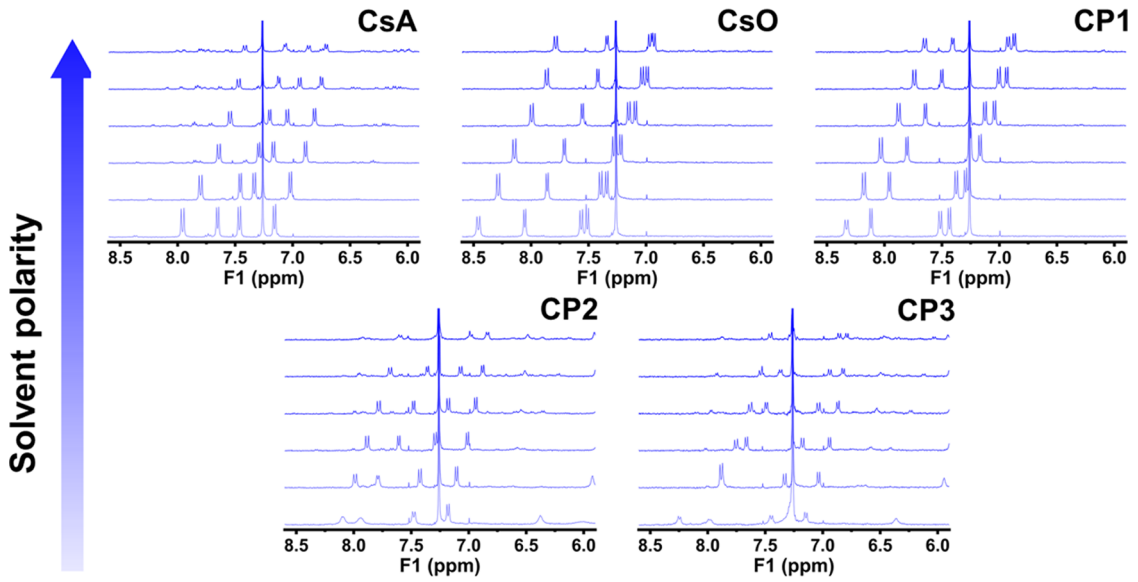

Figure 4. DMSO titration NMR spectra of CsO derivatives obtained by the sequential addition of DMSO-d_6 up to 250 μL in 50 μL increments into 500 μL of $CDCl_3$.

(Tables S10–S12). In **CsA**, the replacement of MeVal[11] with MeLeu[11] had a minimal effect on backbone conformation.[48] This was also the case in **CsO**, and **CP1** showed a conformation similar to **CsO** (Figure 3c). We confirmed that the conformational ensembles of undecameric cyclic peptides, **CsA**, **CsO**, and **CP1**, could be calculated with several significant interactions derived from NMR spectra, and their backbone conformations were predicted to be similar in the nonpolar environment. In the cases of **CP2** and **CP3**, the calculation failed to generate converged ensemble conformations. NMR spectroscopic data of **CP2** and **CP3** indicated intrinsic conformational heterogeneity and the absence of intramolecular hydrogen bonds, suggesting that these are crucial factors that limit the utility of molecular simulation of macrocyclic peptide conformation.

Conformational Changes Depending on Environmental Polarity. The conformational changes depending on the environmental polarity, namely, molecular chameleonicity, have been experimentally examined using NMR spectroscopy (Figure 4).[42] Although **CsA**, **CsO**, and **CP1** showed similar closed conformations in the nonpolar environment through 2D NMR spectroscopy and molecular simulation, they showed different patterns of conformational changes in the dimethyl sulfoxide (DMSO) titration experiment (Figure 4). As the polarity increased with the sequential additions of DMSO, the 1D ^{1}H spectra of **CsA** showed multiple minor peaks, which resulted from minor conformations. Unlike **CsA**, **CsO** and **CP1** appeared to maintain a single conformation in the range of solvent polarity examined. As mentioned above in the VT and HDX-NMR experiments (Figures S29 and S30), **CP2** and **CP3** exhibited broad NMR peaks in $CDCl_3$, and multiple minor conformers appeared as the solvent polarity increased, indicating less defined and more heterogeneous conformations. Therefore, it is difficult to clearly interpret the conformational changes in **CP2** and **CP3** with increasing polarity.

PAMPA Permeability Evaluation. Permeability under passive diffusion was determined using PAMPA (Table 3). **CsO** exhibited 7-fold lower permeability than **CsA**, and **CP1** showed 5-fold lower permeability than **CsO**. Previously, some cyclosporine derivatives showed decreased membrane permeability compared to **CsA**.[14] Additional hydrogen bonds, polar functional groups, and acetyl modifications were detrimental to the membrane permeability of cyclosporines. Similar to the above cases, such differences may impact the membrane permeability of **CsO** and **CP1**. **CP2** and **CP3** are nonpermeable cyclic peptides relative to their counterparts without Gln[7]. Its flexible conformation in the hydrophobic environment and polar side chain of Gln[7] have hampered permeation through the artificial membrane.

Table 3. PAMPA Permeability and Lipophilicity of CsO Derivatives

compound	permeability ($\times 10^{-6}$ cm/s)[a]	R (%)[b]	AlogP[c]
Cz	11 ± 1		
CsA	1.97 ± 0.23	87 ± 1	4.333
CsO	0.29 ± 0.09	84 ± 9	4.765
CP1	0.06 ± 0.01	74 ± 4	5.154
CP2	<0.004	60 ± 1	3.840
CP3	<0.009	75 ± 1	4.228

[a]Permeability was determined by PAMPA. [b]R(%): mass retention. [c]AlogP was calculated with Discovery Studio v.17.1. Cz, carbamazepine.

In vitro membrane permeability was evaluated for **CsO** and **CP1–3** using Caco-2 cells (Table 4). The Caco-2 cell monolayer is a cell line used to represent the intestinal epithelium for the evaluation of the apparent permeability of drugs.[66] Drugs can permeate the Caco-2 cell monolayer by the transcellular pathway, the paracellular pathway, or active transporters. The Caco-2 membrane permeability of **CsA**, **CsO**, and **CP1** was consistent with their membrane permeability as determined by PAMPA. Their similar membrane permeability indicated that they permeate the cell membrane with the same mechanism, namely, the transcellular pathway under passive diffusion. However, they exhibited a different efflux ratio, which is an indicator of whether a molecule is a substrate or inhibitor of P-glycoprotein (P-gp). Although **CsA** is a well-known substrate and inhibitor of P-gp, **CsO** and **CP1** showed efflux ratios (ER = 10 and 9, respectively) close to that of loperamide, a representative P-

https://doi.org/10.1021/acs.jmedchem.1c00211
J. Med. Chem. 2021, 64, 8272–8286

Table 4. Caco-2 Permeability and Percent Recovery of CsO Derivatives

	Caco-2 permeability assay						
	AtoB		BtoA			AtoB with verapamil	
compound	permeability ($\times 10^{-6}$ cm/s)	% recovery	permeability ($\times 10^{-6}$ cm/s)	% recovery	efflux ratio (ER)	permeability ($\times 10^{-6}$ cm/s)	% recovery
CsA	1.51 ± 0.30	58 ± 6	4.51 ± 1.14*	52 ± 1*	3	2.50 ± 0.30	68 ± 6
CsO	0.29 ± 0.05	82 ± 3	2.88 ± 0.97	82 ± 17	10	0.69 ± 0.19	123 ± 3
CP1	0.07 ± 0.004	66 ± 21	0.61 ± 0.16	65 ± 8	9	0.34 ± 0.09	107 ± 4
CP2	0.05 ± 0.02	76 ± 2	5.17 ± 0.19	88 ± 6	111	0.07 ± 0.02	112 ± 14
CP3	0.12 ± 0.05	89 ± 2	8.60 ± 1.20	87 ± 6	70	0.18 ± 0.04	110 ± 24
propranolol	20.0 ± 2.7	121 ± 8	20.4 ± 9.3*	157 ± 2*	1	25.7 ± 4.5	101 ± 7
atenolol							
loperamide	2.9 ± 2.0	88 ± 6	27.5 ± 1.6	85 ± 1	10	5.1 ± 1.1	78 ± 1

Caco-2 permeability assay was carried out in triplicate. A 10 μM sample was dissolved in 1% (v/v) DMSO/HBSS solution, and 100 μM verapamil in Hank's balanced salt solution (HBSS) buffer solution was used as a P-glycoprotein inhibitor. Inserts with Caco-2 cells were preincubated at 37 °C with verapamil for 30 min and then incubated at 37 °C for 2 h without shaking. The efflux ratio was calculated as AtoB permeability/BtoA permeability. Aliquots (20 μL) were collected at each time point (0.5, 1, 1.5, 2 h). *Experiment was carried out in duplicate. The efflux ratio was determined as AtoB permeability/BtoA permeability.

gp substrate. This indicates that **CsO** and **CP1** are pumped out of cells by efflux protein as P-gp substrates without inhibition. **CP2** and **CP3** were evaluated in PAMPA as poorly membrane-permeable cyclic peptides but exhibited comparable permeability with **CP1** and **CsO**, respectively, in Caco-2 permeability assay. They showed a higher efflux ratio than **CsA** by 1 or 2 orders of magnitude (ER = 111 and 70, respectively). Different permeation mechanisms (e.g., the paracellular route[28] or by active transporter[24]) other than passive diffusion may contribute to the permeation of **CP2** and **CP3** through the cell membrane along with being pumped out by efflux proteins.

***In Vivo* Pharmacokinetic Study.** For the evaluation of *in vivo* pharmacokinetic profiles, **CsA** and **CsO** were injected into male ICR mice via intravenous (iv, 5 mg/kg) and oral (po, 20 mg/kg) administration routes (Figure 5). **CsO** showed a higher plasma concentration than **CsA** after intravenous injection. In addition, the plasma concentration of **CsA** went below the lower limit of quantification after 15 min. It has been acknowledged that analyses of the pharmacokinetic profile of **CsA**, a well-known cyclophilin binder, are complicated by the high expression of CypA in red blood cells (e.g., erythrocytes).[52,67] In the blood-to-plasma partitioning experiment, **CsA** showed a 5-fold higher blood-to-plasma partitioning ratio (BPR) than **CsO** at a 1 μM dose (BPR = 3.12 versus 0.62 for **CsA** and **CsO**, respectively) and a similar BPR to **CsO** as the dose increased (Figure 6). The higher BPR of **CsA** indicated a preferential accumulation in red blood cells, which caused the lower plasma concentration, while the preferential accumulation of **CsO** in plasma was explained by BPR < 1 at all dosages, which led to higher plasma concentrations. After oral administration, **CsO** and **CsA** were rapidly absorbed and exhibited nearly the same T_{max}, indicating absorption by the same mechanism (Figure 5). **CsO** showed moderate oral bioavailability (F = 12 ± 0.3%); however, the oral bioavailability of **CsA** could not be obtained due to the low plasma concentration after iv injection. The previously reported PK data for **CsA** indicated an oral bioavailability in the range of 20−30%.[34,39,68,69] The discrepancy in the plasma exposure and oral bioavailability could be explained by the formulation conditions. The self-emulsifying drug delivery system (SEDDS)[70] optimized for **CsA** formulation (e.g., Neoral or Sandimmun) was used for the previous mouse or rat PK studies,[34,39,68,69] suggesting the impact of appropriate vehicle to formulate lipophilic compounds. The PK data shown in Figure 5 can be varied for **CsA** and **CsO** employing the optimized SEDDS, and further follow-up studies are warranted.

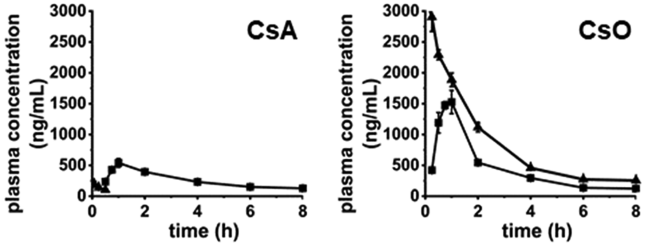

Figure 5. Pharmacokinetic plasma concentration−time curves following iv (5 mg/kg, ▲) and po (20 mg/kg, ■) administration of **CsA** and **CsO**. **CsA**: po, T_{max} = 1.0 h, $AUC_{\infty,po}$ = 2900 ± 100 ng·h/mL, C_{max} = 540 ± 70 ng/mL, CL = 117 ± 6 mL/min/kg, V_z = 46.7 ± 0.6 L/kg, $t_{1/2}$ = 4.6 ± 0.3 h, F = NA; **CsO**: iv, $AUC_{\infty,iv}$ = 8500 ± 400 ng/h/mL, CL = 9.8 ± 0.5 mL/min/kg, V_{ss} = 4.0 ± 0.4 L/kg, $t_{1/2}$ = 4.8 ± 0.6 h; po, T_{max} = 0.8 ± 0.1 h, $AUC_{\infty,po}$ = 4080 ± 50 ng·h/mL, C_{max} = 1600 ± 100 ng/mL, CL = 82 ± 1 mL/min/kg, V_z = 22.2 ± 0.7 L/kg, $t_{1/2}$ = 3.1 ± 0.1 h, F = 12 ± 0.3%. NA, not applicable.

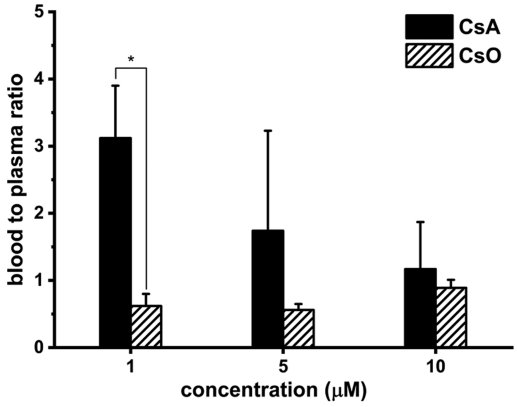

Figure 6. Blood-to-plasma ratios versus injected concentrations of **CsA** and **CsO**. Error bars represent standard deviations. Statistical significance was determined using Student's t test (*p < 0.05).

Cyclophilin A inhibition. The inhibitory constant against CypA was determined using an uncoupled peptidyl-prolyl

https://doi.org/10.1021/acs.jmedchem.1c00211
J. Med. Chem. 2021, 64, 8272−8286

isomerase functional assay (Table 5).[71] **CsO** and **CP1−3** showed weaker binding to CypA than **CsA**, and **CP1** and **CP3** had no inhibitory effect up to 20 μM (Figure S17). **CsO** exhibited approximately 330-fold lower binding affinity to CypA than **CsA**. It was demonstrated that the β-hydroxyl group of the MeBmt residue is crucial to stabilize the binding conformation of **CsA** to CypA through the formation of an intramolecular hydrogen bond with 4CO, and the lower binding affinity of **CsO** to CypA can be rationalized.[60] A comparable inhibitory constant to that of **CsO** was observed in **CP2**, meaning Gln^7 substitution was less relevant to binding CypA. For MeLeu^{11}-substituted cyclic peptides, **CP1** and **CP3**, no inhibitory action could be explained by the cocrystal structure of the CsA-CypA-calcineurin complex (PDB no.: 1MF8). In the complex, buried MeVal^{11} was found in a compact pocket on the surface of CypA, explaining that side-chain variations at position 11 affected the binding to CypA. Several cyclosporines derivatized at position 11 lost their immunosuppressive activity as well.[48] This strongly supported that MeVal^{11} was a fine-tuned residue that bound to CypA tightly, but Gln^7 had no significant effect on CypA binding.

Table 5. Inhibitory Constants of CsO Derivatives against CypA

compound	K_i (μM)
CsA	0.007 ± 0.003
CsO	2.3 ± 0.9
CP1	>20
CP2	3.0 ± 1.4
CP3	>20

DISCUSSION

Aqueous solubility and cell permeability are two key determinants for a compound to have pharmaceutical utility. Both properties are primarily dependent on the balance between polar and nonpolar structures within the compound. In the small-molecule chemical space, Lipinski's Rule of Five provides a guideline to meeting the appropriate polar-nonpolar balance using cLogP, number of hydrogen-bond donors and acceptors, and molecular weight.[72] PSA has also been suggested as another important guideline for meeting the drug-likeness criteria (e.g., <140 Å^2).[73] As the size of a molecule increases, it becomes more difficult to achieve polar-nonpolar balance, so compounds with molecular weights greater than 1000 Da often suffer from poor aqueous solubility (i.e., too nonpolar) or lack of membrane permeability through passive diffusion (i.e., too polar). Some molecules in this bRo5 chemical space exhibit an interesting conformational feature to get around this problem. They change their conformation depending on environmental polarity, exposing polar groups in aqueous media (open conformation), but masking them during the passage through the lipid membrane (closed conformation).[37,74] This type of conformational flexibility is called molecular chameleonicity.

In macrocyclic scaffolds, chameleonicity has emerged as an important contributor to achieving membrane permeability and aqueous solubility.[75] This unique property has been observed in some natural products[35] and synthetic molecules,[38] but we still lack an understanding of which structural determinants or design principles should be used to exploit chameleonicity in macrocycles, particularly for those macrocycles with molecular weights greater than 1000 Da. Hence, various molecular scaffolds in this chemical space have been systematically investigated to measure the degree of impact of flexibility and rigidity on membrane permeability.[23,37,39,76]

CsA has attracted interest in biological applications for decades and has recently been reinvestigated as a representative chameleonic macrocycle.[35] In general, CsA derivatives show high membrane permeability, but it is reduced when polarity is increased or chameleonic behavior is lost. Comparing **CsA**, CsC (Abu^2 → Thr^2), and CsE (MeVal^{11} → Val^{11}) (Figure S19) provides an example. CsC has one added polar −OH substituent and shows somewhat reduced permeability ($\log P_{e,CsA} = -5.01$ versus $\log P_{e,CsC} = -5.56$).[14] CsE has the unmethylated −NH group at MeVal^{11} and is known to be the least permeable among cyclosporines ($\log P_{e,CsE} = -6.38$).[14] Along with the increased polarity of the added hydrogen-bond donor, conformational features of CsE can be changed as well. With an additional hydrogen bond between 11NH and 8CO, CsE showed a similar closed conformation in the hydrophobic environment but lower chameleonic behavior than **CsA**.[77] This more rigid conformation is less favorable to transitioning to the open conformation, leading to membrane permeability that is one-twentieth that of **CsA**.

CsO exhibited weaker chameleonicity than **CsA** during the transition between hydrophobic and aqueous environments despite the similarly closed conformation in the hydrophobic environment. We suggest that the membrane permeability of **CsO** is reduced by the lack of chameleonicity, considering that its lipophilicity, pattern of intramolecular hydrogen bonds, and lipophilic conformation are similar to those of **CsA**. In **CsO**, the decrease in chameleonic behavior was due to side-chain variation: MeLeu^1 and Nva^2 in **CsO** instead of MeBmt^1 and Abu^2 in **CsA**. The replacement of Abu with Nva would have a lower impact on the modulation of chameleonicity because the relevant CsA derivatives in which one carbon is different in position 2 (e.g., cyclosporin B and D; see Figure S19) show no significant change in hydrogen-bonding patterns or in membrane permeability.[14] Thus, the side chain of the residue at position 1 would substantially contribute to the modulation of the extent of chameleonicity of cyclosporines. Macrocycles with noticeable chameleonic behavior often contain long and flexible side chains, which contribute to conformational switching.[38,76] The β-hydroxyl group of MeBmt^1 in **CsA** forms an intramolecular hydrogen bond with 1CO in nonpolar environments,[61] supporting the crucial role of the MeBmt^1 residue in the chameleonicity of **CsA** and rationalizing the reduced chameleonicity of **CsO**. These observations hint at the structural requirements that induce chameleonicity. Although Gln^7, as a long side chain, can also induce the chameleonicity of cyclosporines, the conformational transition was obscured by the disruption of the closed conformation in the nonpolar environment. Determining the nature of the closed conformation is a prerequisite to addressing the structural requirements for chameleonicity.

A recent report by Lokey and co-workers indicated that both rigid and chameleonic macrocyclic peptides (i.e., libraries A and B, respectively) showed high membrane permeability.[23] Other rigid macrocycles, such as rifampicin[76] and cyclic hexapeptides[39] also demonstrated membrane permeability and oral bioavailability. An *in vivo* PK evaluation of **CsO**, a macrocycle that is more rigid than **CsA**, exhibited an approximately 2- or 3-fold decrease in oral bioavailability (F

https://doi.org/10.1021/acs.jmedchem.1c00211
J. Med. Chem. 2021, 64, 8272−8286

= 12 ± 0.3%), while the PAMPA permeability decrease was 7-fold compared to **CsA**. Our results and those of Lokey, Kihlberg, and Fairlie suggest that, for macrocycles with a molecular weight greater than 1000 Da, chameleonicity may not be an absolute prerequisite for achieving acceptable oral bioavailability. However, the flexible and nonchameleonic scaffolds **CP2** and **CP3** exhibited poor membrane permeability, and our separate study indicated a poor PK profile for the CP3 derivative (data not shown). Their heterogeneous conformations in the hydrophobic environment and the polar side chain Gln^7 entail high enthalpic and entropic costs for transit into the membrane. **CP2** and **CP3** have to remove the adjacent water molecules that mask the polar glutamine side chain and experience unfavorable interactions with the lipid membrane. In addition, their flexible conformations are restricted to a well-organized lipid layer. These factors cause decreased accumulation in the membrane, leading to limited membrane permeation of **CP2** and **CP3**. Taken together, a rigid conformation in the hydrophobic environment and an avoidance of polar side chains are required before pursuing chameleonicity to achieve high membrane permeability. In addition, a small variation in the side chain of a macrocycle often results in a major impact: a substitution by polar side chains can cause deleterious effect on membrane permeability and oral bioavailability.[34,78]

Conformational rigidity (or flexibility) affects protein binding and biological functions. The CsO scaffold showed a more than 1000-fold reduced binding affinity to CypA compared to **CsA**. **CsA** adopts an open conformation when bound to CypA,[79] meaning the conformation of **CsA** must transform into an open conformation in aqueous media to bind CypA. The weak chameleonicity of **CsO**, or the less favored transition to an open conformation leads to its low binding affinity. In addition, the binding affinity to CypA explains the discrepancy in the plasma concentrations of **CsA** and **CsO**. CypA is notably overexpressed in red blood cells compared to other cells or tissues,[80] and **CsA** can preferentially accumulate in red blood cells when administered into whole blood. This explanation is consistent with clinical pharmacokinetic profiles;[81] the plasma concentration of **CsA** achieved after oral administration was higher than that achieved after intravenous injection with the formulation conditions used in our study. As a weak CypA binder, **CsO** exhibited higher plasma exposure, a beneficial aspect in terms of pharmacokinetics, and can be expected to have fewer immune-related side effects.

The major side effect of **CsA** in long-term clinical use is nephrotoxicity.[82] Although the reason for the adverse effect has not been clearly explained in the molecular level, it is believed that the intrinsic hydrophobicity of **CsA** or reactive oxygen species (ROS) generation induced by **CsA** in the renal cells could play a significant role. We compared the cytotoxicity of **CsA** and **CsO** against renal cell lines (Table S14). No dramatic difference in cytotoxicity was observed, likely due to the hydrophobic nature of both peptides; however, we did observe that **CsO** was slightly less toxic than **CsA** against kidney epithelial cell lines (e.g., MDCK and BSC-1; Table S14). Along with the lack of CypA binding, the cytotoxicity data suggest the potential utility of CsO derivatives that can overcome the suboptimal pharmacology and potential side effects of **CsA**. Beyond the structural and pharmacokinetic properties of **CsO**, understanding the biological characteristics of **CsO** compared to **CsA** is crucial for the biomedical application of CsO derivatives, which certainly calls for further study.

CONCLUSIONS

Our study provides a deeper understanding of **CsO**, an attractive macrocyclic scaffold for diversity generation, and insights into the relationship between the conformation and permeability of these cyclosporine macrocycles. In particular, we propose the substitution of $MeBmt^1$ in **CsA** to $MeLeu^1$ in **CsO** was a major contributor for the distinct behavior of the two in terms of structure, solubility in aqueous and nonpolar environment, and therefore permeability. Although **CsA** and **CsO** exhibited similar patterns of intramolecular hydrogen bonds and backbone conformations in the hydrophobic environment, the nature of their intramolecular hydrogen bonds differs. In **CsO** and **CP1**, a rigid β-sheet with the hydrogen bonds of 2NH−5CO and 5NH−2CO is better maintained and stabilized compared to **CsA**. The more rigid and less chameleonic conformation of **CsO** resulted in reduced membrane permeability relative to **CsA**. On the other hand, the rigid conformation of **CsO** resulted in weaker binding to CypA, leading to more plasma exposure in the PK profile and less unwanted immunomodulatory activity involving calcineurin binding. In the CsO scaffold, polar Gln^7 substitution resulted in conformational heterogeneity with disrupted transannular hydrogen bonds and detrimental effects on membrane permeability. At this point, we cannot conclude that the CsO scaffold is not tolerable to any polar side-chain incorporation in terms of the maintenance of a closed conformation and membrane permeability. A more systematic study of polar amino acid incorporation at sites other than seventh residue, where the intramolecular hydrogen bond of 8NH-6CO may be disrupted by a long side chain, and the effects on conformation and membrane permeability is warranted. Further modifications and studies of the SPR of the CsO scaffold will indicate structural requirements or insights on how to exploit chameleonicity in macrocycles. We believe that a closed conformation in nonpolar environments in the presence of polar side chains can be formed in this chemical space. This may constitute a significant advancement in the generation of design principles in these macrocycles for orally bioavailable drugs targeting intracellular PPIs.

EXPERIMENTAL SECTION

Materials. Reagents and solvents were purchased from commercial vendors and used without further purification. Rink amide MBHA resin and 2-chlorotrityl resin were purchased from Novabiochem (Darmstadt, Germany). Fmoc-MeVal-OH, Fmoc-Val-OH, and Fmoc-Nva-OH were purchased from Advanced ChemTech (Louisville, KY). HATU and HOAt were purchased from Chem-Impex International, Inc. (Wood Dale, IL). TFA, DMF (>99.9%, for peptide synthesis grade), and dithiothreitol (DTT) were purchased from Acros Organics (Fair Lawn, NJ). Acetonitrile (HPLC grade) was purchased from Fisher Scientific (Waltham, MA). **CsA**, Fmoc-Ala-OH, Fmoc-D-Ala-OH, Fmoc-Leu-OH, (+)-10-camphorsulfonic acid, *p*-formaldehyde, DIC, DIEA, LiCl, and 1,2-dierucosyl-*sn*-glycero-3-phosphocholine were purchased from Tokyo Chemical Industry (Tokyo, Japan). Deuterated solvents were purchased from Cambridge Isotopes Laboratories (Tewksbury, MA). CypA was purchased from R&D Systems (Minneapolis, MN). HBSS buffer was purchased from Gibco (Carlsbad, CA). Dulbecco's modified Eagle's medium (DMEM) buffer was purchased from Welgene (Gyeongsan, Korea). Suc-Ala-Ala-Pro-Phe-*p*-nitroanilide, MultiScreen 96-well plates for PAMPA assay (MAIPNTR10 and PATRNPS50), other reagents and solvents were purchased from Sigma-Aldrich (St. Louis, MO). Empty

https://doi.org/10.1021/acs.jmedchem.1c00211
J. Med. Chem. 2021, 64, 8272−8286

cartridge, frit, and cap plugs were purchased from Applied Separations (Allentown, PA). HTS Transwell 96-well plates (Product no.: 3381) for Caco-2 permeability assay were purchased from Corning (Corning, NY).

Reversed-Phase HPLC. Analytical HPLC was performed on a Waters HPLC system (Waters 2489 UV−visible detector, Waters 1525 binary HPLC pump, Waters 2707 autosampler, and Water 5CH column oven) with a C18 column (SunFire, C18, 4.6 × 250 mm^2, 5 μm). The column oven temperature was set at 40 °C. The binary mobile phase was used as follows: A, water with 0.1% CF_3COOH; B, CH_3CN with 0.1% CF_3COOH; flow rate, 1 mL/min; (1) 0−5 min at 50% B, 5−25 min with a linear gradient to 100% B, and 25−30 min at 100% B for **CsO**; (2) 0−5 min at 70% B, 5−25 min with a linear gradient to 100% B, 25−30 min at 100% B for **CP1**; and (3) 0−5 min at 10% B, 5−25 min with a linear gradient to 100% B, and 25−30 min at 100% B for **CP2** and **CP3**. Peptides were monitored at 220 and 254 nm. Preparative HPLC was performed on a Waters HPLC system (Waters prepLC system, Waters 2545 quaternary HPLC pump, Waters 2489 UV−visible detector, Waters fraction collector III) with a C18 column (SunFire, C18, 19 × 150 mm^2, 5 μm) at a flow rate of 14 mL/min. Preparative HPLC was performed under the same mobile phase conditions as analytical HPLC, and sample elution was monitored at 220 and 254 nm by absorbance. Fractions with >97% purity were collected, lyophilized, and stored at −80 °C.

LC-MS. LC-MS analysis was performed on an Agilent Technology Infinity 1260 system (quaternary pump, autosampler, temperature controller, and Hewlett Packard series 1100 detector) and Agilent 6120 quadrupole MS with a C18 column (Poroshell, 120 EC-C18, 4.6 × 50 mm^2, 2.7 μm). The column heating temperature was set at 50 °C. A binary mobile phase system was used as follows: A, water with 0.1% CF_3COOH; B, CH_3CN with 0.1% CF_3COOH; flow rate, 0.8 mL/min; 0−2 min at 5% B, 2−7 min with a linear gradient to 100% B, and 7−10 min at 100% B. Peptides were monitored at 220 and 254 nm.

Peptide Synthesis. Cyclic peptides were synthesized manually via a standard Fmoc/^{t}Bu solid-phase peptide synthesis (SPPS) protocol. Reactions were accelerated by microwave heating, and a CEM MARS multimodal microwave reactor equipped with a fiber-optic temperature probe and magnetic stirrer was used (CEM Corp., Matthews, NC). For the synthesis of **CsO** and **CP1**, 2-chlorotritylchloride resin (110 mg, 0.13 mmol, loading 1.14 mmol/g) was swelled in CH_2Cl_2 (3 mL) at room temperature for 20 min. Fmoc-Ala-OH (120 mg, 0.39 mmol, 3.0 equiv) in CH_2Cl_2 (2 mL) was added, followed by DIEA (140 mg, 0.78 mmol, 6.0 equiv), and the resin was stirred at room temperature for 5 h. The resin was washed with CH_2Cl_2 (×2), DMF (×2), MeOH (×1), DMF (×2), and CH_2Cl_2 (×2). For Fmoc deprotection, the resin was treated with 20% (v/v) piperidine/DMF solution (2 mL) at room temperature for 5 min and then washed using the above sequence. Amino acid coupling was performed by the addition of Fmoc-amino acid (0.39 mmol, 3.0 equiv), HATU (150 mg, 0.39 mmol, 3.0 equiv), and DIEA (130 mg, 1.04 mmol, 8.0 equiv) in DMF (2 mL). The mixture was stirred under microwave irradiation (75 °C, 300 W max power, ramp 2.5 min, hold 8.0 min, stirring level 3) and washed using the above sequence. Coupling reactions were employed twice for MeLeu^{10}−D-Ala^8 to improve the total yield. Fmoc deprotection and amino acid coupling were repeated until the desired linear peptide was obtained. The coupling reaction of MeLeu^{10} onto MeVal^{11} for **CsO** was performed by the addition of Fmoc-MeLeu-OH (140 mg, 0.39 mmol, 3.0 equiv), HOAt (53 mg, 0.39 mmol, 3.0 equiv), DIC (49 mg, 0.39 mmol, 3.0 equiv), and DIEA (100 mg, 0.39 mmol, 3.0 equiv) in DMF (2 mL) and was repeated twice. The linear peptide was cleaved with TFA/TIS/CH_2Cl_2 95:2.5:2.5 (v/v/v) at room temperature for 10 min. The volatiles were evaporated using a stream of N_2 gas, and the crude peptide was dissolved in 1:1 (v/v) water/acetonitrile solution, filtered, lyophilized, and used for the cyclization reaction without further purification. The linear peptide (~0.13 mmol) was dissolved in DMF (125 mL) containing DIEA (340 mg, 2.6 mmol, 20 equiv), and the solution was stirred at room temperature for 30 min to facilitate free amine formation at the N-terminus. HATU (250 mg, 0.65 mmol, 5.0 equiv) in DMF (5 mL) was added to the mixture, and the concentration of peptide was kept at 1.0 mM. The mixture was stirred under microwave irradiation (75 °C, 300 W max power, ramp 2.5 min, hold 17.5 min, stirring level 3). The mixture was then cooled to room temperature, and the reaction was quenched by water. The solvent was evaporated under reduced pressure (50 mbar) at 75 °C. The residue was dissolved in 1:1 (v/v) water/acetonitrile, filtered by a 0.45 μm poly(tetrafluoroethylene) (PTFE) syringe filter, and purified by preparative HPLC to obtain **CsO** and **CP1**. Purity confirmed by analytical HPLC (220 nm) is >98% for **CsO** and **CP1**. For the synthesis of **CP2** and **CP3**, Fmoc-Rink amide MBHA resin (250 mg, 0.13 mmol, loading 0.52 mmol/g) was used. After Fmoc deprotection, the resin was treated with Fmoc-Glu-OAll (160 mg, 0.39 mmol, 3.0 equiv), HATU (150 mg, 0.39 mmol, 3.0 equiv), and DIEA (130 mg, 1.04 mmol, 8.0 equiv) in DMF (2 mL) and stirred under microwave irradiation (75 °C, 300 W max power, ramp 2.5 min, hold 8.0 min, stirring level 3). After peptide elongation, allyl deprotection was carried out by the addition of $Pd(PPh_3)_4$ (15 mg, 0.013 mmol, 0.1 equiv) and $PhSiH_3$ (340 mg, 3.1 mmol, 24 equiv) in CH_2Cl_2 (2 mL) at room temperature for 3 h. The N-terminal Fmoc was removed after allyl deprotection by treatment with 20% (v/v) piperidine/DMF solution (2 mL). The resin was thoroughly washed between each reaction using the above conditions. For the on-resin macrocyclization, the resin was swelled in CH_2Cl_2 (2 mL) for 20 min. PyBOP (270 mg, 0.52 mmol, 4.0 equiv), HOAt (70 mg, 0.52 mmol, 4.0 equiv), and DIEA (168 mg, 1.3 mmol, 10 equiv) in CH_2Cl_2 (2 mL) were added to the resin, and the mixture was stirred at room temperature for 2 h. The resin was washed, and the cyclic peptide was cleaved from the resin using TFA/TIS/CH_2Cl_2 95:2.5:2.5 (v/v/v) at room temperature for 2 h. The cleavage solution was concentrated using a stream of N_2 gas. The residue was dissolved in 1:1 (v/v) water/acetonitrile, filtered, and purified by preparative HPLC to yield **CP2** and **CP3**. Purities are confirmed by analytical HPLC (220 nm) for **CP2** and **CP3** are 97 and 98%, respectively. Electrospray ionization mass spectrometry (ESI-MS) m/z **CsO**: calcd for $C_{60}H_{110}N_{11}O_{11}$ $[M + H]^+$ 1160.8, found 1160.7; **CP1**: calcd for $C_{61}H_{112}N_{11}O_{11}$ $[M + H]^+$ 1174.9, found 1174.7; **CP2**: calcd for $C_{62}H_{113}N_{12}O_{12}$ $[M + H]^+$ 1217.9, found 1217.7; **CP3**: calcd for $C_{63}H_{115}N_{12}O_{12}$ $[M + H]^+$ 1231.9, found 1231.8.

NMR Spectroscopy. All NMR experiments were carried out using a JEOL 400 MHz (GIST, Gwangju) or a Bruker 900 MHz NMR spectrometer equipped with the cryoprobe (KBSI, Ochang). 1D ^{1}H spectra were collected at 298−318 K on a JEOL 400 MHz NMR spectrometer, and 2D NMR spectra including heteronuclear single quantum coherence (HSQC), heteronuclear multiple bond correlation (HMBC), total correlated spectroscopy (TOCSY), and NOESY were obtained at 298 K on a Bruker 900 MHz NMR spectrometer. The samples for 2D NMR spectra were prepared at 2 mg/mL. 2D NMR data processing and analysis were performed by Topspin (Bruker) and SPARKY software, respectively.[83] For variable-temperature NMR spectroscopy, each cyclic peptide (3 mg) was dissolved in $CDCl_3$ (500 μL), and 1D ^{1}H NMR spectra were measured at 5 K intervals between 298 and 318 K. The chemical shift changes of amide protons were recorded to calculate the temperature coefficients for each amide proton.[84] For hydrogen-deuterium exchange NMR spectroscopy, each cyclic peptide (3 mg) was dissolved in 9:1 (v/v) $CDCl_3/CD_3OD$ (500 μL).[26] CD_3OD was used as a source of exchangeable deuterium, and 1D ^{1}H NMR spectra were measured at 298 K at eight time points (0, 30, 60, 120, 180, 360, 720, and 1440 min). The integration of peaks corresponding to amide protons was carried out compared with a proton signal of tetramethylsilane as an internal standard to calculate the H/D exchange rate of the amide protons. For DMSO-titrated NMR spectroscopy, each cyclic peptide (3 mg) was dissolved in $CDCl_3$ (500 μL), and 1D ^{1}H NMR spectra were measured at 298 K with every 50 μL addition of DMSO-d_6 up to 250 μL. The chemical shift changes of each amide proton were recorded depending on the volume percentage of DMSO-d_6.

Generation of Conformational Ensemble. The conformations of cyclic peptides were predicted through a previously reported method, Conformational Analysis from NMR and Density functional prediction of Low-energy Ensembles (CANDLE),[65] which employs

https://doi.org/10.1021/acs.jmedchem.1c00211
J. Med. Chem. 2021, 64, 8272−8286

molecular dynamics simulations and quantum mechanical calculations. For molecular dynamics simulations, the CHARMM force field was applied to an initial geometry with MMFF94 for partial charge estimation. High-temperature molecular dynamics (HTMD) simulations were performed at 2000 K for 60 ns with a 1 fs time step by Discovery Studio v17.1 (BIOVIA, CA) to cover as many diverse backbone conformations as possible. The dielectric constant was set to that of chloroform ($\varepsilon = 4.8$) under the Born implicit solvent model to mimic the hydrophobic environment. A total of 12 000 conformations were generated with snapshots taken every 5 ps (6000 conformations for **CsA**), and then rational conformations were selected by NOE-based assignments for amide bonds (<|45°| for cis or >|135°| for trans). In HTMD, a single determinant of the amide bond was used because the conformation was too flexible to allow consideration of the distance constraints at 2000 K. The selected conformations were clustered by the dihedral angles (φ and ψ) of all amino acids in a backbone with a cluster level of 20. The single-point energy of each conformation was calculated with B3LYP/6-31G(d) via Gaussian09. The lowest single-point energy conformation from 20 clusters was adopted for geometry optimization with M062X/6-31G(d) in a gas phase. Among them, the lowest-energy conformation was used as a seed conformation for room-temperature molecular dynamics (RTMD) simulations.

RTMD simulations were conducted at 300 K for 60 ns with a 1 fs time step by Discovery Studio v17.1. The snapshots that were taken every 10 ps generated 6000 conformations. The conformations were selected by significant interactions derived from NOE spectra corresponding to the distance (distance ≤ 3.5 Å). The single-point energy of selected conformations was calculated with B3LYP/6-31G(d), and geometry optimization was performed with M062X/6-31G(d) for 20 low-energy conformations. The lowest-energy conformation in each RTMD simulation was used as a seed conformation for the next RTMD simulation. RTMD simulations and geometry optimization were repeated until no lower-energy conformer was obtained. The population for each conformation was calculated by the Boltzmann energy distribution ($N = Ae^{-\Delta E/RT}$), and conformations representing at least 1% of the population were collected and superimposed as a representative ensemble of conformations.

Parallel Artificial Membrane Permeability Assay (PAMPA).[13,21] PAMPA was conducted with a 96-well donor plate with 0.45 μm hydrophobic immobilon-P membrane supports and a 96-well polystyrene acceptor plate in triplicate. A 1% (w/v) solution of lecithin in *n*-dodecane was prepared and sonicated for 5 min before being used for PAMPA. Lecithin solution (5 μL) was carefully added into each membrane support in the bottom of the donor plate without the pipet tip touching the membrane. Each sample was prepared as a 10 μM solution in 5% (v/v) DMSO/phosphate-buffered saline (PBS) buffer. The donor plates were prepared by the addition of a sample solution (150 μL), and the acceptor plates were filled with 5% DMSO/PBS buffer (300 μL). The donor plate was placed on top of the acceptor plate without any bubbles between the donor and acceptor plates. A lid was placed on the donor plate, and the whole plates were covered with a wet paper towel to prevent evaporation. Then, the plates were incubated for 18 h at room temperature. Next, an aliquot (50 μL) from each donor or acceptor was mixed with 50 μM Fmoc-Tyr(O*t*Bu)-OH dissolved in 1:1 (v/v) water/acetonitrile (50 μL) as an internal standard. The mixture (30 μL) was injected into the LC-MS instrument, and the analyte and internal standard were monitored in selected ion monitoring (SIM) mode. The analyte-to-standard peak area ratios were calculated and used to determine the relative concentrations. These concentrations were used to calculate the mass retention (R) and permeability (P_e)

$$R = 1 - \left(\frac{C_d \times V_d + C_a \times V_a}{C_0 \times V_d}\right)$$

$$P_e = \frac{V_a \times V_d}{V_0 \times A \times t} \times \ln\left(1 - \frac{C_a}{C_{eq}}\right)\left(C_{eq} = \frac{C_d \times V_d + C_a \times V_a}{V_d + V_a}\right)$$

wherer C_0 is the initial concentration of donor plate (10 μM), C_a is the concentration of acceptor plate (μM), C_d is the concentration of donor plate (μM), V_a is the volume of acceptor plate (300 μL), V_d is the volume of donor plate (150 μL), A is the area of membrane (0.24 cm^2), t is the time (s), and $V_0 = V_a + V_d$.

Caco-2 Permeability Assay. Caco-2 cells (passage 33−34) were incubated in DMEM (pH 7.3) containing 10% fetal bovine serum, 100 U/mL penicillin, and 100 μg/mL streptomycin. The cells were grown in 100-mm tissue culture Petri dishes (Eppendorf AG, Hamburg, Germany) and maintained in an atmosphere of 5% CO_2 and 90% relative humidity at 37 °C. For Caco-2 permeability assay, 2.5×10^5 Caco-2 cells/well were seeded into each insert in an HTS Transwell 96-well plate. The cells were incubated on the inserts in DMEM for 3 weeks, and the culture medium was replaced with fresh medium every 3 days until the whole area of the membrane was covered. After 21 days, the inserts and the plate were washed twice with HBSS buffer (pH 7.4) and incubated in fresh HBSS buffer at 37 °C for 1 h (120 μL was dispensed into the inserts and 250 μL into the receiver plate). For apical to basolateral (AtoB) permeability with verapamil, the cells were preincubated in HBSS buffer containing verapamil (200 μM, 60 μL) for 30 min before permeability assay. After the HBSS buffer was drained, the sample solution (10 μM in 1% DMSO/HBSS) was added to the inserts (120 μL) or the receiver plate (250 μL). For AtoB permeability with verapamil, the sample solution (20 μM in 2% DMSO/HBSS) was added to the inserts (60 μL). The opposite side was filled with HBSS buffer. AtoB permeability, BtoA permeability, and AtoB permeability with verapamil were measured to evaluate the apparent permeability, permeation pathway, and efflux ratio, respectively. The well plate was incubated at 37 °C without shaking for 2 h. Aliquots (20 μL) taken at each time point (0.5, 1, 1.5, 2 h) were mixed with Fmoc-Tyr(O*t*Bu)-OH in acetonitrile solution (60 μL) as internal standards. The mixture was centrifuged at 1000 rpm for 15 min and then analyzed by LC-MS in selected ion monitoring (SIM) mode. Each experiment was performed in triplicate. In addition, aliquots of the donor were taken at 2 h to calculate the recovery (%). The analyte-to-standard peak area ratio was calculated and used to determine permeability (P_{app}) and recovery (%)

$$P_{app} = \frac{dQ}{dt} \times \frac{1}{A \times C_0}$$

$$\text{recovery}(\%) = \frac{C_d + C_{2h}}{C_0} \times 100$$

where dQ/dt is the permeability rate (cm/s), A is the area of insert (0.143 cm^2), C_0 is the initial concentration (10 μM), C_d is the concentration of donor at 2 h (μM), C_{2h} is the concentration of acceptor at 2 h (μM).

Caco-2 monolayers and tight junctions were confirmed by a test using Lucifer yellow, which could not pass through Caco-2 cells. After permeability assay, Caco-2 cells were incubated in HBSS buffer at 37 °C for 1 h for the Lucifer yellow assay. The inserts were filled with Lucifer yellow solution in HBSS buffer (60 μM, 75 μL), and a receiver plate was prepared by HBSS buffer (235 μL). The plate was incubated at 37 °C for 1 Hyposmocoma lucifer yellow passage (%) was determined by monitoring fluorescence at 530 nm (excitation: 480 nm). Inserts that showed less than 3% Lucifer yellow passage were valid for permeability assay.

Animals. Male ICR mice (9 weeks old, 33−37 g) were purchased from Koatec (Pyeongtaek, South Korea) and used for the pharmacokinetic and blood-to-plasma partitioning studies. Experimental protocols involving the animals used in this study were reviewed and approved by the Institutional Animal Care and Use Committee of Korea Research Institute of Bioscience and Biotechnology (KRIBB-AEC-19275, approved on January 3, 2020).

Mouse Plasma Pharmacokinetic Study. Pharmacokinetic studies of **CsA** and **CsO** were conducted in male ICR mice. Dosing solutions (dimethylacetamide/Tween 80/20% 2-hydropropyl-β-cyclodextrin 1:1:8 (v/v/v)) containing either **CsA** or **CsO** were

https://doi.org/10.1021/acs.jmedchem.1c00211
J. Med. Chem. 2021, 64, 8272−8286

administered intravenously by injection via the tail vein (5 mg/kg, 5 mL/kg) or administered orally by gavage (20 mg/kg, 10 mL/kg). Blood samples were collected at 0.08, 0.25, 0.5, 1, 2, 4, 6, 8, and 24 h (intravenous administration) or at 0.25, 0.5, 0.75, 1, 2, 4, 6, 8, and 24 h (oral administration) via the saphenous vein. The plasma fraction was separated from the blood samples by centrifugation (12000*g* for 5 min at 4 °C) and subjected to protein precipitation by the addition of 4 volumes of acetonitrile. After vigorous vortexing and centrifugation (2000*g* for 10 min at 4 °C), an aliquot of the supernatant was collected and injected into LC-MS/MS.

Blood-to-Plasma Partitioning Study. Mouse fresh whole blood was taken from male ICR mice in heparin-containing tubes immediately prior to the experiment. Following 10 min of preincubation in a 37 °C water bath, whole blood was spiked with stock solutions of **CsA** and **CsO** dissolved in acetonitrile (0.1, 0.5, 1 mg/mL) to reach final concentrations of 1, 5, and 10 μg/mL. In parallel, fresh mouse plasma prepared from the same batch of fresh whole blood was spiked with identical volumes of stock solutions. The mixtures were then incubated at 37 °C for 60 min, and plasma fractions from whole blood were collected by centrifugation (2000*g* for 10 min at 4 °C) at the end of incubation. Subsequently, chilled acetonitrile (180 μL) was added to the generated plasma and reference plasma samples (60 μL) for protein precipitation. After vigorous vortexing and centrifugation (2000*g* for 10 min at 4 °C), an aliquot of the supernatant was collected and injected into the LC-MS/MS.

The partition coefficients of **CsA** and **CsO** in red blood cells were calculated as follows

$$K_{\mathrm{RBC/PL}} = \frac{1}{H}\cdot\left(\frac{I_{\mathrm{PL}}^{\mathrm{REF}}}{I_{\mathrm{PL}}} - 1\right) + 1$$

$$K_{\mathrm{B/P}} = (K_{\mathrm{RBC/PL}} \times H) + (1 - H)$$

where $K_{\mathrm{RBC/PL}}$ is the partition coefficient of a given drug in red blood cells over that in equilibrating plasma, H is hematocrit, $I_{\mathrm{PL}}^{\mathrm{REF}}$ and I_{PL} are the peak areas of the reference plasma sample and equilibrating plasma sample, respectively, and $K_{\mathrm{B/P}}$ is the partition coefficient of blood over plasma.

LC-MS/MS Analysis of Pharmacokinetic and Blood Cell Partitioning Study Samples. The bioanalytical assays for pharmacokinetic and red blood cell partitioning studies were carried out using an API3200 mass spectrometer (Applied Biosystems, Toronto, Canada) equipped with an API electrospray ionization source. The elution was carried out using a linear gradient from 2 to 98% MeOH in water at a flow rate of 0.4 mL/min with a reversed-phase liquid chromatography column (Xterra MS C18, 2.1 × 50 mm^2, 5 μm; Waters, Milford, MA). The temperature of the column oven was maintained at 40 °C during the analysis, and the multiple reaction monitoring data were collected in positive ionization mode. The analytes were monitored at the following Q1/Q3 transitions (m/z): 1203.1 → 425.5 for **CsA** and 1161.2 → 156.2 for **CsO**. Data acquisition and quantitation were performed using Analysis software v1.5.2 (Applied Biosystems, Toronto, Canada).

Peptidyl-prolyl Isomerase Functional Assay. The assay was performed using a Jasco model 810 spectropolarimeter (Jasco, Inc., Easton, MD) as described in a previously reported protocol.[71] *N*-(2-hydroxyethyl)piperazine-*N*′-ethanesulfonic acid (HEPES) buffer (35 mM, pH 7.8) with 50 μM DTT and 8 nM cyclophilin A was cooled to 10 °C. An inhibitor in 100% DMSO stock solution (20 μL) was added into the buffer (1960 μL), and the mixture was incubated at 10 °C for 15 min. The tetrapeptide substrate Suc-Ala-Ala-Pro-Phe-*p*-nitroanilide dissolved in 0.5 M LiCl in trifluoroethanol (6 mM, 20 μL) was added to the mixture. The change in absorbance was measured over 5 min at 330 nm with an optical path length of 10 mm. A first-order rate equation was fitted to the absorbance data to evaluate an observed rate constant. The catalytic rate constant was calculated from the observed rate constant minus the background rate constant. The catalytic rate constant was plotted against inhibitor concentration, and it was fitted using the Morrison K_i equation to obtain an inhibitory constant (K_i) for each inhibitor

$$Y = Y_0 \times \frac{E - [I] - K_i + \sqrt{(E - [I] - K_i)^2 + 4 \times E \times K_i}}{2 \times E}$$

where Y_0 is the rate constant in the absence of inhibitor, E is the concentration of enzyme (8 nM), $[I]$ is the concentration of inhibitor, and K_i is the inhibitory constant.

■ ASSOCIATED CONTENT

Supporting Information

The Supporting Information is available free of charge at https://pubs.acs.org/doi/10.1021/acs.jmedchem.1c00211.

HPLC data; 2D NMR; VT NMR; HDX-NMR; CD spectra; computational details; solubility measurement; and cyclophilin A binding assay (Figures S1−S19 and Tables S1−S14) (PDF)

Molecular formula strings (CSV)

Coordinates for calculated conformation of CsA (PDB)

Coordinates for calculated conformation of CsO (PDB)

Coordinates for calculated conformation of CP1 (PDB)

■ AUTHOR INFORMATION

Corresponding Authors

Chin-Ju Park − *Department of Chemistry, Gwangju Institute of Science and Technology (GIST), Gwangju 61005, Republic of Korea;* orcid.org/0000-0002-7750-1554; Email: cjpark@gist.ac.kr

Kyeong-Ryoon Lee − *Laboratory of Animal Resource Center, Korea Research Institute of Bioscience and Biotechnology (KRIBB), Ochang 28116, Republic of Korea;* orcid.org/0000-0003-2175-8876; Email: kyeongrlee@kribb.re.kr

Jun-Ho Choi − *Department of Chemistry, Gwangju Institute of Science and Technology (GIST), Gwangju 61005, Republic of Korea;* orcid.org/0000-0001-5237-5566; Email: junhochoi@gist.ac.kr

Jiwon Seo − *Department of Chemistry, Gwangju Institute of Science and Technology (GIST), Gwangju 61005, Republic of Korea;* orcid.org/0000-0002-5433-5071; Email: jseo@gist.ac.kr

Authors

Dongjae Lee − *Department of Chemistry, Gwangju Institute of Science and Technology (GIST), Gwangju 61005, Republic of Korea*

Sungjin Lee − *Department of Chemistry, Gwangju Institute of Science and Technology (GIST), Gwangju 61005, Republic of Korea*

Jieun Choi − *Department of Chemistry, Gwangju Institute of Science and Technology (GIST), Gwangju 61005, Republic of Korea*

Yoo-Kyung Song − *Laboratory of Animal Resource Center, Korea Research Institute of Bioscience and Biotechnology (KRIBB), Ochang 28116, Republic of Korea*

Min Ju Kim − *Laboratory of Animal Resource Center, Korea Research Institute of Bioscience and Biotechnology (KRIBB), Ochang 28116, Republic of Korea*

Dae-Seop Shin − *Bio Platform Technology Research Center, Korea Research Institute of Chemical Technology (KRICT), Daejeon 34114, Republic of Korea*

Myung Ae Bae − *Bio Platform Technology Research Center, Korea Research Institute of Chemical Technology (KRICT), Daejeon 34114, Republic of Korea*

Yong-Chul Kim − *School of Life Sciences, Gwangju Institute of Science and Technology, Gwangju 61005, Republic of Korea;* orcid.org/0000-0003-1520-2011

Complete contact information is available at: https://pubs.acs.org/10.1021/acs.jmedchem.1c00211

Notes

The authors declare no competing financial interest.

■ ACKNOWLEDGMENTS

This research was financially supported by the Korea Health Industry Development Institute (KHIDI) (HI16C1074 to J.S.), the National Research Foundation of Korea (NRF-2021R1A2C2014421 and 2018M3D1A1052659 to J.S., 2018R1D1A1B07042015 to J.-H.C.), a "GIST Research Institute (GRI)" grant funded by the GIST in 2021 (J.S.), and a grant received from Korea Research Institute of Bioscience and Biotechnology (KRIBB) Research Initiative Programs (KGS9982022 to K.-R.L.). The work was funded in part by the Korea Basic Science Institute (KBSI, Ochang) under its R&D program (project no. D38700 to C.-J.P.), which is supervised by the Ministry of Science and ICT, Korea. The authors thank the high-field NMR facility at KBSI for enabling our NMR experiments.

■ ABBREVIATIONS

Abu, aminobutyric acid; BTC, bis(trichloromethyl)carbonate; BPR, blood-to-plasma ratio; CANDLE, conformational analysis from NMR and density functional prediction of low-energy ensembles; CsA, cyclosporin A; CsO, cyclosporin O; CypA, cyclophilin A; DIC, *N*,*N*′-diisopropylcarbodiimide; DIEA, *N*,*N*-diisopropylethylamine; HATU, 1-[bis-(dimethylamino)methylene]-1*H*-1,2,3-triazole[4,5-*b*]-pyridinium 3-oxide hexafluorophosphate; HOAt, 1-hydroxy-7-azabenzotriazole; HTMD, high-temperature MD; MeBmt, (4*R*)-4-[(*E*)-2-butenyl]-4-methyl-L-threonine; MeLeu, *N*-methylated leucine; MeVal, *N*-methylated valine; NOE, nuclear Overhauser effect; Nva, norvaline; PPIs, protein−protein interactions; PyBOP, (benzotriazol-1-yloxy)-tripyrrolidinophosphonium hexafluorophosphate; RP-HPLC, reversed-phase-high-performance liquid chromatography; RTMD, room-temperature MD; SPPS, solid-phase peptide synthesis; SPR, structure−permeability relationship; TIS, triisopropylsilane; TOCSY, total correlated spectroscopy

■ REFERENCES

(1) Arkin, M. R.; Tang, Y.; Wells, J. A. Small-molecule inhibitors of protein−protein interactions: progressing toward the reality. *Chem. Biol.* **2014**, *21*, 1102−1114.
(2) Arkin, M. R.; Wells, J. A. Small-molecule inhibitors of protein−protein interactions: progressing towards the dream. *Nat. Rev. Drug Discovery* **2004**, *3*, 301−317.
(3) Smith, M. C.; Gestwicki, J. E. Features of protein−protein interactions that translate into potent inhibitors: topology, surface area and affinity. *Expert Rev. Mol. Med.* **2012**, *14*, No. e16.
(4) Villar, E. A.; Beglov, D.; Chennamadhavuni, S.; Porco, J. A.; Kozakov, D.; Vajda, S.; Whitty, A. How proteins bind macrocycles. *Nat. Chem. Biol.* **2014**, *10*, 723−731.
(5) Qian, Z.; Dougherty, P. G.; Pei, D. Targeting intracellular protein−protein interactions with cell-permeable cyclic peptides. *Curr. Opin. Chem. Biol.* **2017**, *38*, 80−86.
(6) Doak, B. C.; Zheng, J.; Dobritzsch, D.; Kihlberg, J. How beyond rule of 5 drugs and clinical candidates bind to their targets. *J. Med. Chem.* **2016**, *59*, 2312−2327.
(7) Doak, B. C.; Over, B.; Giordanetto, F.; Kihlberg, J. Oral druggable space beyond the rule of 5: insights from drugs and clinical candidates. *Chem. Biol.* **2014**, *21*, 1115−1142.
(8) Hill, T. A.; Shepherd, N. E.; Diness, F.; Fairlie, D. P. Constraining cyclic peptides to mimic protein structure motifs. *Angew. Chem., Int. Ed.* **2014**, *53*, 13020−13041.
(9) Gavenonis, J.; Sheneman, B. A.; Siegert, T. R.; Eshelman, M. R.; Kritzer, J. A. Comprehensive analysis of loops at protein-protein interfaces for macrocycle design. *Nat. Chem. Biol.* **2014**, *10*, 716−722.
(10) Luther, A.; Moehle, K.; Chevalier, E.; Dale, G.; Obrecht, D. Protein epitope mimetic macrocycles as biopharmaceuticals. *Curr. Opin. Chem. Biol.* **2017**, *38*, 45−51.
(11) Hruby, V. J.; al-Obeidi, F.; Kazmierski, W. Emerging approaches in the molecular design of receptor-selective peptide ligands: conformational, topographical and dynamic considerations. *Biochem. J.* **1990**, *268*, 249−262.
(12) Qian, Z.; Rhodes, C. A.; McCroskey, L. C.; Wen, J.; Appiah-Kubi, G.; Wang, D. J.; Guttridge, D. C.; Pei, D. Enhancing the cell permeability and metabolic stability of peptidyl drugs by reversible bicyclization. *Angew. Chem.* **2017**, *129*, 1547−1551.
(13) Rezai, T.; Yu, B.; Millhauser, G. L.; Jacobson, M. P.; Lokey, R. S. Testing the conformational hypothesis of passive membrane permeability using synthetic cyclic peptide diastereomers. *J. Am. Chem. Soc.* **2006**, *128*, 2510−2511.
(14) Ahlbach, C. L.; Lexa, K. W.; Bockus, A. T.; Chen, V.; Crews, P.; Jacobson, M. P.; Lokey, R. S. Beyond cyclosporine A: conformation-dependent passive membrane permeabilities of cyclic peptide natural products. *Future Med. Chem.* **2015**, *7*, 2121−2130.
(15) Kling, A.; Lukat, P.; Almeida, D. V.; Bauer, A.; Fontaine, E.; Sordello, S.; Zaburannyi, N.; Herrmann, J.; Wenzel, S. C.; König, C.; et al. Targeting DnaN for tuberculosis therapy using novel griselimycins. *Science* **2015**, *348*, 1106−1112.
(16) Bockus, A. T.; Schwochert, J. A.; Pye, C. R.; Townsend, C. E.; Sok, V.; Bednarek, M. A.; Lokey, R. S. Going out on a limb: delineating the effects of *β*-branching, N-methylation, and side chain size on the passive permeability, solubility, and flexibility of sanguinamide A analogues. *J. Med. Chem.* **2015**, *58*, 7409−7418.
(17) Schwochert, J.; Lao, Y.; Pye, C. R.; Naylor, M. R.; Desai, P. V.; Gonzalez Valcarcel, I. C.; Barrett, J. A.; Sawada, G.; Blanco, M.-J.; Lokey, R. S. Stereochemistry balances cell permeability and solubility in the naturally derived phepropeptin cyclic peptides. *ACS Med. Chem. Lett.* **2016**, *7*, 757−761.
(18) Hewitt, W. M.; Leung, S. S.; Pye, C. R.; Ponkey, A. R.; Bednarek, M.; Jacobson, M. P.; Lokey, R. S. Cell-permeable cyclic peptides from synthetic libraries inspired by natural products. *J. Am. Chem. Soc.* **2015**, *137*, 715−721.
(19) Ono, S.; Naylor, M. R.; Townsend, C. E.; Okumura, C.; Okada, O.; Lokey, R. S. Conformation and permeability: cyclic hexapeptide diastereomers. *J. Chem. Inf. Model.* **2019**, *59*, 2952−2963.
(20) Schwochert, J.; Turner, R.; Thang, M.; Berkeley, R. F.; Ponkey, A. R.; Rodriguez, K. M.; Leung, S. S.; Khunte, B.; Goetz, G.; Limberakis, C.; et al. Peptide to peptoid substitutions increase cell permeability in cyclic hexapeptides. *Org. Lett.* **2015**, *17*, 2928−2931.
(21) Furukawa, A.; Townsend, C. E.; Schwochert, J.; Pye, C. R.; Bednarek, M. A.; Lokey, R. S. Passive membrane permeability in cyclic peptomer scaffolds is robust to extensive variation in side chain functionality and backbone geometry. *J. Med. Chem.* **2016**, *59*, 9503−9512.
(22) Biron, E.; Chatterjee, J.; Ovadia, O.; Langenegger, D.; Brueggen, J.; Hoyer, D.; Schmid, H. A.; Jelinek, R.; Gilon, C.; Hoffman, A.; Kessler, H. Improving oral bioavailability of peptides by multiple N-methylation: somatostatin analogues. *Angew. Chem., Int. Ed.* **2008**, *47*, 2595−2599.
(23) Furukawa, A.; Schwochert, J.; Pye, C. R.; Asano, D.; Edmondson, Q. D.; Turmon, A. C.; Klein, V. G.; Ono, S.; Okada, O.; Lokey, R. S. Drug-like properties in macrocycles above MW 1000: backbone rigidity versus side-chain lipophilicity. *Angew. Chem., Int. Ed.* **2020**, *59*, 21571−51577.

(24) Marelli, U. K.; Bezençon, J.; Puig, E.; Ernst, B.; Kessler, H. Enantiomeric cyclic peptides with different caco-2 permeability suggest carrier-mediated transport. *Chem. - Eur. J.* **2015**, *21*, 8023−8027.
(25) Lohman, R.-J.; Nielsen, D. S.; Kok, W. M.; Hoang, H. N.; Hill, T. A.; Fairlie, D. P. Mirror image pairs of cyclic hexapeptides have different oral bioavailabilities and metabolic stabilities. *Chem. Commun.* **2019**, *55*, 13362−13365.
(26) Nielsen, D. S.; Hoang, H. N.; Lohman, R. J.; Hill, T. A.; Lucke, A. J.; Craik, D. J.; Edmonds, D. J.; Griffith, D. A.; Rotter, C. J.; Ruggeri, R. B.; et al. Improving on nature: making a cyclic heptapeptide orally bioavailable. *Angew. Chem., Int. Ed.* **2014**, *53*, 12059−12063.
(27) Fouché, M.; Schäfer, M.; Berghausen, J.; Desrayaud, S.; Blatter, M.; Piéchon, P.; Dix, I.; Martin Garcia, A.; Roth, H. J. Design and development of a cyclic decapeptide scaffold with suitable properties for bioavailability and oral exposure. *ChemMedChem* **2016**, *11*, 1048−1059.
(28) Schumacher-Klinger, A.; Fanous, J.; Merzbach, S.; Weinmüller, M.; Reichart, F.; Räder, A. F.; Gitlin-Domagalska, A.; Gilon, C.; Kessler, H.; Hoffman, A. Enhancing oral bioavailability of cyclic RGD hexa-peptides by the lipophilic prodrug charge masking approach: redirection of peptide intestinal permeability from a paracellular to transcellular pathway. *Mol. Pharm.* **2018**, *15*, 3468−3477.
(29) Buckton, L. K.; McAlpine, S. R. Improving the cell permeability of polar cyclic peptides by replacing residues with alkylated amino acids, asparagines, and D-amino acids. *Org. Lett.* **2018**, *20*, 506−509.
(30) Bockus, A. T.; Lexa, K. W.; Pye, C. R.; Kalgutkar, A. S.; Gardner, J. W.; Hund, K. C.; Hewitt, W. M.; Schwochert, J. A.; Glassey, E.; Price, D. A.; et al. Probing the physicochemical boundaries of cell permeability and oral bioavailability in lipophilic macrocycles inspired by natural products. *J. Med. Chem.* **2015**, *58*, 4581−4589.
(31) Naylor, M. R.; Ly, A. M.; Handford, M. J.; Ramos, D. P.; Pye, C. R.; Furukawa, A.; Klein, V. G.; Noland, R. P.; Edmondson, Q.; Turmon, A. C.; et al. Lipophilic permeability efficiency reconciles the opposing roles of lipophilicity in membrane permeability and aqueous solubility. *J. Med. Chem.* **2018**, *61*, 11169−11182.
(32) Pye, C. R.; Hewitt, W. M.; Schwochert, J.; Haddad, T. D.; Townsend, C. E.; Etienne, L.; Lao, Y.; Limberakis, C.; Furukawa, A.; Mathiowetz, A. M.; Price, D. A.; Liras, S.; Lokey, S. R. Nonclassical size dependence of permeation defines bounds for passive adsorption of large drug molecules. *J. Med. Chem.* **2017**, *60*, 1665−1672.
(33) Beck, J. G.; Chatterjee, J.; Laufer, B.; Kiran, M. U.; Frank, A. O.; Neubauer, S.; Ovadia, O.; Greenberg, S.; Gilon, C.; Hoffman, A.; Kessler, H. Intestinal permeability of cyclic peptides: common key backbone motifs identified. *J. Am. Chem. Soc.* **2012**, *134*, 12125−12133.
(34) White, T. R.; Renzelman, C. M.; Rand, A. C.; Rezai, T.; McEwen, C. M.; Gelev, V. M.; Turner, R. A.; Linington, R. G.; Leung, S. S.; Kalgutkar, A. S.; Bauman, J. N.; Zhang, Y.; Liras, S.; Price, D. A.; Mathiowetz, A. M.; Jacobson, M. P.; Lokey, R. S. On-resin N-methylation of cyclic peptides for discovery of orally bioavailable scaffolds. *Nat. Chem. Biol.* **2011**, *7*, 810−817.
(35) Wang, C. K.; Swedberg, J. E.; Harvey, P. J.; Kaas, Q.; Craik, D. J. Conformational flexibility is a determinant of permeability for cyclosporin. *J. Phys. Chem. B* **2018**, *122*, 2261−2276.
(36) Witek, J.; Keller, B. G.; Blatter, M.; Meissner, A.; Wagner, T.; Riniker, S. Kinetic models of cyclosporin A in polar and apolar environments reveal multiple congruent conformational states. *J. Chem. Inf. Model.* **2016**, *56*, 1547−1562.
(37) Whitty, A.; Zhong, M.; Viarengo, L.; Beglov, D.; Hall, D. R.; Vajda, S. Quantifying the chameleonic properties of macrocycles and other high-molecular-weight drugs. *Drug Discovery* **2016**, *21*, 712−717.
(38) Rossi Sebastiano, M.; Doak, B. C.; Backlund, M.; Poongavanam, V.; Over, B.; Ermondi, G.; Caron, G.; Matsson, P. R.; Kihlberg, J. Impact of dynamically exposed polarity on permeability and solubility of chameleonic drugs beyond the rule of 5. *J. Med. Chem.* **2018**, *61*, 4189−4202.
(39) Nielsen, D. S.; Lohman, R. J.; Hoang, H. N.; Hill, T. A.; Jones, A.; Lucke, A. J.; Fairlie, D. P. Flexibility versus rigidity for orally bioavailable cyclic hexapeptides. *ChemBioChem* **2015**, *16*, 2289−2293.
(40) Rezai, T.; Bock, J. E.; Zhou, M. V.; Kalyanaraman, C.; Lokey, R. S.; Jacobson, M. P. Conformational flexibility, internal hydrogen bonding, and passive membrane permeability: successful in silico prediction of the relative permeabilities of cyclic peptides. *J. Am. Chem. Soc.* **2006**, *128*, 14073−14080.
(41) Tyagi, M.; Poongavanam, V.; Lindhagen, M.; Pettersen, A.; Sjö, P.; Schiesser, S.; Kihlberg, J. Toward the design of molecular chameleons: flexible shielding of an amide bond enhances macrocycle cell permeability. *Org. Lett.* **2018**, *20*, 5737−5742.
(42) Efimov, S.; Zgadzay, Y.; Klochkov, V. Observation of conformational exchange in cyclosporin in media of varying polarity by NMR spectroscopy. *Appl. Magn. Reson.* **2014**, *45*, 1225−1235.
(43) Traber, R.; Hofmann, H.; Loosli, H. R.; Ponelle, M.; von Wartburg, A. Neue cyclosporine aus Tolypocladium inflatum. Die cyclosporine K−Z. *Helv. Chim. Acta* **1987**, *70*, 13−36.
(44) Kim, Y.; Yoon, D.-H.; Ha, H.-J.; Kang, K. Y.; Lee, W. K. N-Methylative aziridine ring opening and asymmetric synthesis of MeBmt. *Tetrahedron Lett.* **2011**, *52*, 5918−5920.
(45) Aebi, J. D.; Deyo, D. T.; Sun, C. Q.; Guillaume, D.; Dunlap, B.; Rich, D. H. Synthesis, conformation, and immunosuppressive activities of three analogs of cyclosporin A modified in the 1-position. *J. Med. Chem.* **1990**, *33*, 999−1009.
(46) Rich, D. H.; Sun, C. Q.; Guillaume, D.; Dunlap, B.; Evans, D. A.; Weber, A. E. Synthesis, biological activity, and conformational analysis of (2S, 3R, 4S)-MeBmt-cyclosporin, a novel 1-position epimer of cyclosporin A. *J. Med. Chem.* **1989**, *32*, 1982−1987.
(47) Rich, D. H.; Dhaon, M. K.; Dunlap, B.; Miller, S. P. Synthesis and antimitogenic activities of four analogs of cyclosporin A modified in the 1-position. *J. Med. Chem.* **1986**, *29*, 978−984.
(48) Wenger, R. M. Synthesis of cyclosporine and analogues: structural requirements for immunosuppressive activity. *Angew. Chem., Int. Ed.* **1985**, *24*, 77−85.
(49) Raman, P.; Stokes, S. S.; Angell, Y. M.; Flentke, G. R.; Rich, D. H. Methods to circumvent a difficult coupling in the solid-phase synthesis of cyclosporine analogues. *J. Org. Chem.* **1998**, *63*, 5734−5735.
(50) Ko, S. Y.; Wenger, R. M. Solid-phase total synthesis of cyclosporine analogues. *Helv. Chim. Acta* **1997**, *80*, 695−705.
(51) Kahlert, V.; Prell, E.; Ohlenschläger, O.; Melesina, J.; Schumann, M.; Lücke, C.; Fischer, G.; Marešević, M. Synthesis and biochemical evaluation of two novel N-hydroxyalkylated cyclosporin A analogs. *Org. Biomol. Chem.* **2018**, *16*, 4338−4349.
(52) Sweeney, Z. K.; Fu, J.; Wiedmann, B. From chemical tools to clinical medicines: nonimmunosuppressive cyclophilin inhibitors derived from the cyclosporin and sanglifehrin scaffolds. *J. Med. Chem.* **2014**, *57*, 7145−7159.
(53) Evers, M.; Barrière, J.-C.; Bashiardes, G.; Bousseau, A.; Carry, J.-C.; Dereu, N.; Filoche, B.; Henin, Y.; Sablé, S.; Vuilhorgne, M.; Mignani, S. Synthesis of non-immunosuppressive cyclophilin-binding cyclosporin A derivatives as potential anti-HIV-1 drugs. *Bioorg. Med. Chem. Lett.* **2003**, *13*, 4415−4419.
(54) Thern, B.; Rudolph, J.; Jung, G. Triphosgene as highly efficient reagent for the solid-phase coupling of N-alkylated amino acids—total synthesis of cyclosporin O. *Tetrahedron Lett.* **2002**, *43*, 5013−5016.
(55) Sureshbabu, V. V.; Tantry, S. J.; Chennakrishnareddy, G.; Nagendra, G. Total synthesis of cyclosporin O: exploring the utility of bsmoc-NMe-amino acid fluorides and KOAt. *Protein Peptide Lett.* **2009**, *16*, 312−319.
(56) Tantry, S. J.; Venkataramanarao, R.; Chennakrishnareddy, G.; Sureshbabu, V. V. Total synthesis of cyclosporin O by convergent approach employing Fmoc-amino acid chlorides mediated by zinc dust. *J. Org. Chem.* **2007**, *72*, 9360−9363.
(57) Sewald, N. Efficient, racemization-free peptide coupling of N-alkyl amino acids by using amino acid chlorides generated in situ—

https://doi.org/10.1021/acs.jmedchem.1c00211
J. Med. Chem. 2021, 64, 8272−8286

total syntheses of the cyclopeptides cyclosporin O and omphalotin A. *Angew. Chem., Int. Ed.* **2002**, *41*, 4661−4663.
(58) Li, P.; Xu, J. C. Total synthesis of cyclosporin O both in solution and in the solid phase using novel thiazolium-, immonium-, and pyridinium-type coupling reagents: BEMT, BDMP, and BEP1. *J. Org. Chem.* **2000**, *65*, 2951−2958.
(59) Colucci, W. J.; Tung, R. D.; Petri, J. A.; Rich, D. H. Synthesis of D-lysine8-cyclosporine A. further characterization of BOP-Cl in the 2−7 hexapeptide fragment synthesis. *J. Org. Chem.* **1990**, *55*, 2895−2903.
(60) Angell, Y. M.; Thomas, T. L.; Flentke, G. R.; Rich, D. H. Solid-phase synthesis of cyclosporin peptides. *J. Am. Chem. Soc.* **1995**, *117*, 7279−7280.
(61) Kessler, H.; Köck, M.; Wein, T.; Gehrke, M. Reinvestigation of the conformation of cyclosporin A in chloroform. *Helv. Chim. Acta* **1990**, *73*, 1818−1832.
(62) Cierpicki, T.; Otlewski, J. Amide proton temperature coefficients as hydrogen bond indicators in proteins. *J. Biomol. NMR* **2001**, *21*, 249−261.
(63) Koeck, M.; Kessler, H.; Seebach, D.; Thaler, A. Novel backbone conformation of cyclosporin A: the complex with lithium chloride. *J. Am. Chem. Soc.* **1992**, *114*, 2676−2686.
(64) Loosli, H. R.; Kessler, H.; Oschkinat, H.; Weber, H. P.; Petcher, T. J.; Widmer, A. Peptide conformations. Part 31. The conformation of cyclosporin A in the crystal and in solution. *Helv. Chim. Acta* **1985**, *68*, 682−704.
(65) Nguyen, Q. N. N.; Schwochert, J.; Tantillo, D. J.; Lokey, R. S. Using 1H and 13C NMR chemical shifts to determine cyclic peptide conformations: a combined molecular dynamics and quantum mechanics approach. *Phys. Chem. Chem. Phys.* **2018**, *20*, 14003−14012.
(66) Hidalgo, I. J.; Raub, T. J.; Borchardt, R. T. Characterization of the human colon carcinoma cell line (Caco-2) as a model system for intestinal epithelial permeability. *Gastroenterology* **1989**, *96*, 736−749.
(67) Awni, W.; Sawchuk, R. The pharmacokinetics of cyclosporine. II. Blood plasma distribution and binding studies. *Drug Metab. Dispos.* **1985**, *13*, 133−138.
(68) Lee, Y.-J.; Chung, S.-J.; Shim, C.-K. Limited role of P-glycoprotein in the intestinal absorption of cyclosporin A. *Biol. Pharm. Bull.* **2005**, *28*, 760−763.
(69) Jin, M.; Shimada, T.; Yokogawa, K.; Nomura, M.; Kato, Y.; Tsuji, A.; Miyamoto, K.-I. Contributions of intestinal P-glycoprotein and CYP3A to oral bioavailability of cyclosporin A in mice treated with or without dexamethasone. *Int. J. Pharm.* **2006**, *309*, 81−86.
(70) Neslihan Gursoy, R.; Benita, S. Self-emulsifying drug delivery systems (SEDDS) for improved oral delivery of lipophilic drugs. *Biomed. Pharmacother.* **2004**, 173−182.
(71) Janowski, B.; Wöllner, S.; Schutkowski, M.; Fischer, G. A protease-free assay for peptidyl prolylcis/transisomerases using standard peptide substrates. *Anal. Biochem.* **1997**, *252*, 299−307.
(72) Lipinski, C. A.; Lombardo, F.; Dominy, B. W.; Feeney, P. J. Experimental and computational approaches to estimate solubility and permeability in drug discovery and development settings. *Adv. Drug Delivery Rev.* **1997**, *23*, 3−25.
(73) Veber, D. F.; Johnson, S. R.; Cheng, H.-Y.; Smith, B. R.; Ward, K. W.; Kopple, K. D. Molecular properties that influence the oral bioavailability of drug candidates. *J. Med. Chem.* **2002**, *45*, 2615−2623.
(74) Giordanetto, F.; Kihlberg, J. Macrocyclic drugs and clinical candidates: what can medicinal chemists learn from their properties? *J. Med. Chem.* **2014**, *57*, 278−295.
(75) Ermondi, G.; Vallaro, M.; Goetz, G.; Shalaeva, M.; Caron, G. Updating the portfolio of physicochemical descriptors related to permeability in the beyond the rule of 5 chemical space. *Eur. J. Pharm. Sci.* **2020**, *146*, No. 105274.
(76) Danelius, E.; Poongavanam, V.; Peintner, S.; Wieske, L.; Erdélyi, M.; Kihlberg, J. Solution conformations explain the chameleonic behaviour of macrocyclic drugs. *Chem. - Eur. J.* **2020**, *26*, 5231−5244.
(77) Witek, J.; Mühlbauer, M.; Keller, B. G.; Blatter, M.; Meissner, A.; Wagner, T.; Riniker, S. Interconversion rates between conformational states as rationale for the membrane permeability of cyclosporines. *ChemPhysChem* **2017**, *18*, 3309−3314.
(78) Rand, A. C.; Leung, S. S.; Eng, H.; Rotter, C. J.; Sharma, R.; Kalgutkar, A. S.; Zhang, Y.; Varma, M. V.; Farley, K. A.; Khunte, B.; et al. Optimizing PK properties of cyclic peptides: the effect of side chain substitutions on permeability and clearance. *MedChemComm* **2012**, *3*, 1282−1289.
(79) Mikol, V.; Kallen, J.; Pflügl, G.; Walkinshaw, M. D. X-ray Structure of a monomeric cyclophilin A-cyclosporin A crystal complex at 2.1 Å resolution. *J. Mol. Biol.* **1993**, *234*, 1119−1130.
(80) Ryffel, B.; Woerly, G.; Greiner, B.; Haendler, B.; Mihatsch, M.; Foxwell, B. Distribution of the cyclosporine binding protein cyclophilin in human tissues. *Immunology* **1991**, *72*, 399.
(81) Legg, B.; Gupta, S.; Rowland, M.; Johnson, R.; Solomon, L. Cyclosporin: pharmacokinetics and detailed studies of plasma and erythrocyte binding during intravenous and oral administration. *Eur. J. Clin. Pharm.* **1988**, *34*, 451−460.
(82) Lee, J. Use of antioxidants to prevent cyclosporine a toxicity. *Toxicol. Res.* **2010**, *26*, 163−170.
(83) Lee, W.; Tonelli, M.; Markley, J. L. NMRFAM-SPARKY: enhanced software for biomolecular NMR spectroscopy. *Bioinformatics* **2015**, *31*, 1325−1327.
(84) Wang, C. K.; Northfield, S. E.; Colless, B.; Chaousis, S.; Hamernig, I.; Lohman, R.-J.; Nielsen, D. S.; Schroeder, C. I.; Liras, S.; Price, D. A.; Fairlie, D. P.; Craik, D. J. Rational design and synthesis of an orally bioavailable peptide guided by NMR amide temperature coefficients. *Proc. Natl. Acad. Sci. U.S.A.* **2014**, *111*, 17504−17509.

https://doi.org/10.1021/acs.jmedchem.1c00211
J. Med. Chem. 2021, 64, 8272−8286